# Automotive LiDAR Technology: A Survey

Ricardo Roriz, Jorge Cabral, and Tiago Gomes

***Abstract*— Nowadays, and more than a decade after the first steps towards autonomous driving, we keep heading to achieve fully autonomous vehicles on our roads, with LiDAR sensors being a key instrument for the success of this technology. Such advances trigger the emergence of new players in the automotive industry, and along with car manufacturers, this sector represents a multibillion-dollar market where everyone wants to take a share. To understand recent advances and technologies behind LiDAR, this article presents a survey on LiDAR sensors for the automotive industry. With this work, we show the measurement principles and imaging techniques currently being used, going through a review of commercial systems and development solutions available in the market today. Furthermore, we highlight the current and future challenges, providing insights on how both research and industry can step towards better LiDAR solutions.**

***Index Terms*— Autonomous vehicles, LiDAR, 3D imaging, ToF.**

## I. Introduction

LIGHT-BASED measuring techniques were firstly used in calculating the air density in the upper atmosphere just by reading the intensity of a searchlight beam's reflection. Later, and instead of using continuous light beams, the cloud-base height measurement was obtained by calculating the time taken by a light pulse to travel to the cloud and back to the ground [1]. Back in 1953, Middleton and Spilhaus introduced the Light Detection and Ranging (LiDAR) as a range measuring technique [2], which was initially a portmanteau of the terms light and Radar [3]. However, only with the invention of new techniques such as Dennis Gabor's holography method in 1945 and the laser in 1960 [4], the LiDAR principle was introduced as we know it nowadays: it can measure distances by simply calculating the round-trip time of a laser pulse traveled to the target and back [5]. Nonetheless, and since E.D Hinkley has published his LiDAR textbook in 1976 [6], the evolution of LiDAR has been primarily associated with the improvement of hardware components and measuring techniques, rather than the development of new disrupting measuring principles [7].

Some LiDAR characteristics such as the wavelength, power consumption, pulse width, optical filters, and computing capabilities (LiDAR systems often require extensive data processing), keep pushing forward the technological innovation in areas such as electronics, embedded processing, and optics. In terms of setup [7], a LiDAR sensor is composed of two main components: (1) a transmitter, which consists of a laser that emits light with wavelengths between 250 to 1600 nanometers (nm) - some wavelengths work better in specific environments and targets than others; and (2) a receiver, which is responsible for gathering, analyze, and compute the reflected signal. Regarding the receiver, it generally includes: (a) a telescope to collect the photons; (b) an optical analyzer that can filter specific wavelengths or polarization states from the received light and convert the optical signal into an electrical quantity; and (c) a data acquisition module, which is responsible for calculating the elapsed pulse time and storing the information.

Over the years, LiDAR sensors have been strongly established in a broad range of areas, such as Topography [8], Geoscience [9], Atmospheric [10], and Robotics [11]. However, its first remarkable application in the automotive sector was around the year 2004. For the first time, the Defense Advanced Research Projects Agency (DARPA) announced the Grand Challenge, which consisted in creating fully autonomous vehicles that could navigate desert trails and roads. This challenge emerged as a response to a congressional mandate that demanded a third of US military ground vehicles to be unmanned by 2015 [12]. Despite none of the participants being able to complete the challenge, the vehicle that went furthest in the competition provided a great benchmark for the autonomous driving research [13], exposing some flaws of Camera-based systems and putting LiDAR sensors in the spotlight. The requirement for a real-time obstacle avoidance system turned LiDAR-based sensors almost mandatory [13]. Consequently, in the second edition, five vehicles completed the challenge, being Stanley the first vehicle to achieve 244 km in seven hours [14].

Nowadays, and more than a decade after the first autonomous ride, it is possible to state that we are stepping forward to put fully autonomous vehicles on our roads. The big players in the car industry are already deploying autonomous capabilities in vehicles through advanced driver-assistance systems (ADAS), endowing them with the ability to automatically steer, accelerate, and brake under the driver's active supervision. Such features are continually being improved as new ones are emerging, being LiDAR a key technology for the future of autonomous driving. This represents a multibillion-dollar market that triggers the emergence of new players than just car manufacturers in the automotive sector, a place where everyone wants to take a share. With this work, we present a survey on the automotive LiDAR technology, showing the current technological solutions, major challenges, and recent trends. This article contributes to state of the art with: (1) an overview on LiDAR technology for the automotive industry; (2) the major trends and challenges of this emerging technology; (3) a review of commercial LiDAR systems and development solutions; and (4) the current challenges and important insights on how research and industry can step towards better LiDAR-based solutions.

Manuscript received April 10, 2020; revised November 3, 2020 and May 26, 2021; accepted June 2, 2021. This work was supported by the Fundação para a Ciência e Tecnologia (FCT) within the Research and Development Units Project Scope under Grant UIDB/00319/2020. The Associate Editor for this article was B. Seibold. *(Corresponding author: Tiago Gomes.)*

The authors are with the Centro ALGORITMI, Universidade do Minho, Campus Azurém, 4800-058 Guimarães, Portugal (e-mail: mr.gomes@dei.uminho.pt).

Digital Object Identifier 10.1109/TITS.2021.3086804

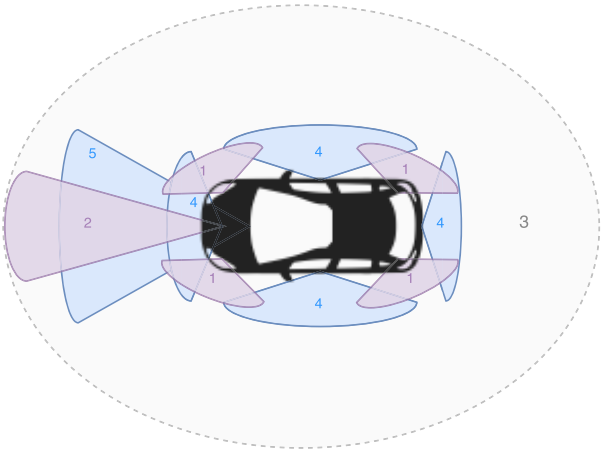


Fig. 1. Autonomous driving multi-sensor setup.

## II. Radar, Cameras, and LiDAR

Currently, autonomous driving features are only possible with multi-sensor data fusion [15]–[18]. To detect the surrounding environment and obstacles, autonomous vehicle perception sensing requires the collection of data from vehicle sensors, with Radar, Camera, and LiDAR being the most prominent technologies in use. Since there is no one-size-fits-all setup for the perception tasks, car manufacturers keep choosing one technology over the others in different combinations, depending on the application requirements and needs. Fig. 1 depicts a setup using all three sensor technologies, which contribute to a better understanding of the world around the vehicle: the Radar provides (1) cross-traffic alerts, blind-spot assisting, and (2) Adaptive Cruise Control; the LiDAR sensor is used to (3) translate the physical world into 3D digital images in real-time and with a high level of confidence; Cameras can help in features such as (4) object detection and classification, and (5) collision avoidance.

The utilization of Cameras has been widely adopted in autonomous vehicles since they provide the most accurate way to create a visual representation of the vehicle's surroundings. Placed on every side of the car, they can retrieve a wide picture of their environment, which can assist the object recognition task. However, the downside of this technology lies in the fact that adverse weather conditions, e.g., fog or rain, or external light sources, can severely affect its output. Moreover, the accurate distance to the surrounding objects needs to be calculated, which is only possible with stereo Cameras or by combining the information from other sensor technologies.

Radar is the most mature technology among the others. Widely used to detect ships and by aircraft vehicles, its reliability and robustness in different environmental conditions is undoubted [19]. Like Cameras, Radar sensors can be placed around the car to detect objects at every angle. Since it works by sending radio wave pulses and reading the returning signal, it allows for an accurate and direct measurement of range, relative velocity (Doppler effect), and the angle of multiple targets without being affected by light conditions. Radar systems for automotive operate in the frequency bands around 24 GHz, 77 GHz, and 79 GHz. While using higher frequency bands can provide higher accuracy for distance and speed measurements and a more precise angular resolution, the 24 GHz can achieve lower interference and use smaller antenna sizes. However, some automotive regulations allow only 1 GHz bandwidth at 77 GHz, making only possible the utilization of 24 GHz systems in short-range applications such as blind spot detection, park assist, cross-traffic monitoring, and object tracking [20], [21], making mid- and long-range applications like automatic distance control or emergency braking hard to perform [22]. Despite being able to determine speed, distances and detect obstacles, they cannot distinguish different types of objects.

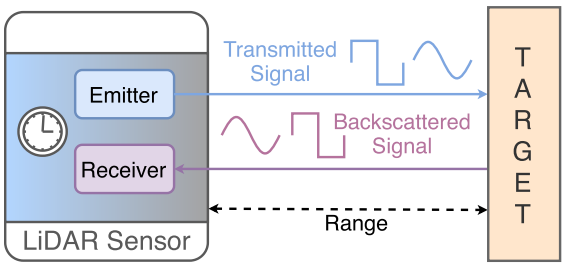


Fig. 2. Operation principle of LiDAR technology.

The utilization of LiDAR sensors in the automotive sector is relatively new, but already getting a lot of attention from car manufacturers. LiDAR technology is assumed as the next step towards full driverless capabilities as it can provide a high resolution and real-time 3D representation (point cloud) of the environment. This representation aims to obtain shape and distance to surrounding cars and pedestrians as well as the road geography, which can also be helpful in object detection and classification. Similarly to Radar, LiDAR sensors have active illumination, which makes them highly effective at night. Because they offer detection ranges up to a few hundred meters, these sensors enrich driverless configurations by filling the existent gap between Radar and Camera technologies.

## III. Basic LiDAR Concepts

The working principle behind the LiDAR technology, Fig. 2, consists in measuring ranges by calculating the round-trip delay of light signals emitted by a laser to a target.

$$R = \frac{1}{2} c\tau \tag{1}$$

The range $R$ to the target can be obtained by using Equation 1, where $c$ is the speed of light, and $\tau$ is the round-trip delay of the emitted signal. The round-trip delay, known as the time of flight (ToF), can be obtained by modulating the frequency, phase, intensity, etc., of the transmitted light and measuring the time for that modulation pattern to be detected at the receiver [23]–[25]. Creating a point cloud, which consists of a 3D representation of the vehicle's environment, requires the ToF to be individually calculated for each point. There are many different measurement and imaging techniques used to help in determining the ToF, which are further

discussed in Sections IV and V, respectively. Regardless of the adopted measurement and imaging techniques, the most important performance metrics for evaluating a LiDAR are its detection range, transmitted power, wavelength, the field of view (FoV), precision, accuracy, resolution, pulse rate, scan rate, and frame rate [25], [26].

### A. Detection Range

The detection range refers to the farthest distance where an object can be detected, which is largely dependent on the sensor's transmitted power. Usually, the range is expressed on its minimum and maximum values, which are obtained and specified in controlled environments by pointing the laser to targets with 80% of diffuse reflectivity. In a real environment, these values can slightly change due to sunlight interference or the target's surface reflectivity.

### B. Transmitted Power

The laser's maximum permissible exposure (MPE), i.e., the maximum laser power allowed, is limited by eye safety regulations. This value is calculated based on the laser's wavelength, beam diameter and motion, duration of exposure for continuous-wave operations, pulse width, and repetition rate for pulsed operations. In applications like autonomous driving, where vehicles and humans coexist, eye safety is mandatory, thus it requires a strong regulation on the transmitted power, which can limit the applicability of LiDAR in terms of range and immunity to noise.

### C. Wavelength

The two wavelengths for automotive LiDAR currently in use are 905 nm, and 1550 nm, making possible light spatial resolution on the order of 0.1 degrees, which allows for extremely high-resolution 3D representation of objects around the vehicle. The 905 nm wavelength was chosen for early LiDAR systems because they are compatible with silicon detector technology and pulsed diode laser emitters were readily available at a very low cost. One drawback of 905 nm lasers is that they fall within the range of wavelengths that can penetrate the eye to the sensitive retina, causing irreversible eye injuries when higher power values are used. Limiting the transmitted power due to eye safety restrictions also limits the 905 nm LiDAR range [27].

Regarding the 1550 nm wavelength, it offers significant advantages in terms of eye safety regulations since the light beyond 1400 nm gets absorbed in the front layers of the eye, mainly because of watery absorption, and does not reach the retina. This enables higher power levels which reflect higher ranges. Therefore, many scanning systems are being designed at this wavelength [28]. However, increasing the transmitted power at this wavelength has its limitations as it can also damage the eye at some power levels. The downside of the 1550 nm is mainly related to the technology used in the 1550 nm emitter/detectors, which require the use of more exotic periodic elements such as Indium Phosphide (InP), Gallium Arsenide (GaAs), and Indium Gallium Arsenide (InGaAs), increasing the overall manufacturing cost. Moreover, environmental conditions, such as rain, fog, and snow, can also limit the performance of a LiDAR sensor, mainly due to water absorption phenomena, which mostly affect the 1550 wavelengths. However, and because the transmitted power can be increased, this wavelength helps LiDAR achieve better performance than the 905 nm [29].

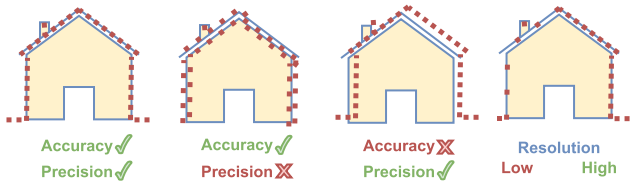


Fig. 3. Precision, accuracy, and resolution of a LiDAR sensor.

### D. Field of View (FoV)

The FoV is defined as the angle in which LiDAR signals are emitted, and for a 3D representation of the vehicle's surroundings, LiDAR sensors must provide both a vertical and horizontal FoV. Additionally, for a full perception of the environment, some sensors can provide a 360° horizontal FoV (HFoV). This can be achieved by using a rotor-based mechanical sensor that spins the scanning part through the entire HFoV, or by combining the output from several sensors with a smaller FoV.

### E. Precision, Accuracy, and Resolution

Precision can be described as the repeatability of the measure, i.e., when different measurements output the same value. Lower precision LiDAR sensors originate noisy point clouds, while precise sensors output a well-defined point cloud. Accuracy is best defined as the geographical precision, i.e., how close a measurement is to the real value. Therefore, an accurate point cloud will be as close as possible to the actual position of the environment it describes. Regarding the resolution of a LiDAR system, it represents the smallest angular or linear separation between two points that can be resolved by the sensor. In other terms, it can be seen as the number of unit pulses per unit area. Therefore, higher resolution sensors are able to create denser point clouds. Fig. 3 illustrates the precision, accuracy, and resolution parameters of a LiDAR sensor.

### F. Pulse, Scan, and Frame Rate

The pulse rate can be defined as the rate at which the sensor measures pulses. This metric characterizes particularly beam-steering sensors, and high pulse rate values usually produce denser point cloud data. Newer systems can also collect multiple returns from the same laser pulse, allowing, for instance, the detection of elevated surfaces. The scan rate corresponds to the time it takes to scan the entire FoV, and it is directly related to the imaging technique used by the sensor, e.g., mechanical or solid-state scanning LiDAR. In flash LiDAR systems the scan rate is often expressed as the frame rate, since their operation is very similar to a standard digital camera and the entire FoV can be captured in a single image measurement.

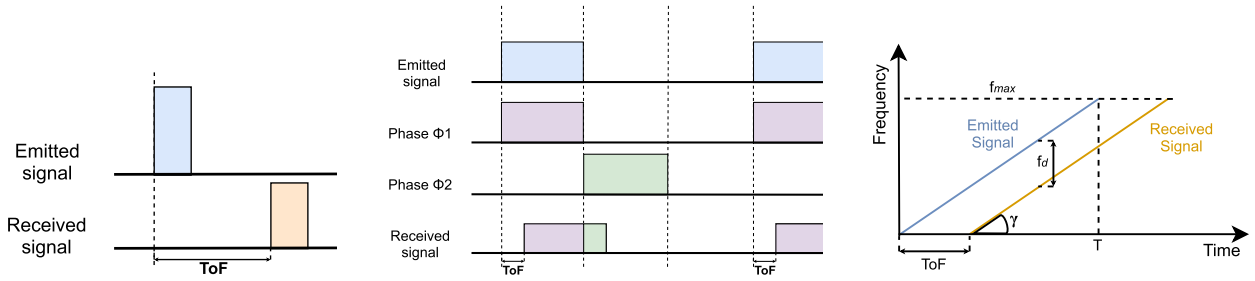


(a) Pulsed Direct ToF. (b) AMCW. (c) FMCW.

Fig. 4. LiDAR measurement approaches.

## IV. LiDAR Measurement Principles

The distance to a target can be calculated through pulsed or continuous wave measurement techniques [30]–[32]. Simple architectures often provide cheaper implementations, however, they usually lack accuracy and are less immune to mutual interference caused by other LiDAR sensors. By their turn, more robust approaches can provide better results, but they usually require complex circuitry and electronic systems.

### A. Pulsed ToF

Measurement techniques based on pulsed ToF, Fig. 4a, use the time interval between the transmitted and received light to calculate the distance to a target. The round-trip delay is obtained by using accurate timers or time-to-digital (TDC) converters [33], which can offer several advantages [34], such as: (1) they are simple to implement; (2) they require low complexity emitter and receiver systems; and (3) they provide a low-cost and small-size solution without complex optical systems, e.g., lenses and extra sensing circuitry. However, simple architectures that use direct ToF can face flickering problems that result in low accuracy measurements, and, due to external light sources caused by mutual interference, the signal-to-noise (SNR) ratio is often low [35]. Attempts to increase the SNR usually require complex and sometimes hardware-costly methods, dictated by eye safety regulations that limit the laser's transmitted power. Short pulse widths can achieve higher peak power while maintaining the eye safety exposure, however, this highly influences the receiver's hardware design.

### B. Amplitude Modulated Continuous Wave (AMCW)

AMCW approaches and pulsed ToF operate in a similar way, however, AMCW schemes do not include sharp pulses. Instead, they transmit continuous optical power modulating the light's intensity [25]. In AMCW systems, the distance is calculated by partitioning the reflected signal over a series of integrating windows. Firstly, the sensor emits a pulse synchronized with the first window, which will be reflected back to the sensor out of phase. After the pulse is transmitted, a second integration window is enabled. Based on the ratio between both windows, which hold fractions of the received light, the ToF can be calculated. For short distances, most of the received light is detected by the first window, while for longer distances the return light is more present in the second window. Fig. 4b depicts the working principle of an AMCW LiDAR sensor [36]. Because AMCW sensors measure optical energy disregarding the wavelength used, they require simple laser systems, which makes the overall sensor's size small. However, since the distance is measured based on the received power, multi-target detection becomes a hard task. Achieving longer ranges would be possible with longer transmitted pulses, which would also decrease the SNR. However, since eye safety regulations limit the transmitting power, this architecture is being mainly deployed in mid- and short-range applications [28], [31].

### C. Frequency Modulated Continuous Wave (FMCW)

FMCW LiDAR systems use wave light properties to calculate distances instead of modulating the intensity of the transmitted signal. The frequency of the emitted signal is linearly modulated in time with an up-chirp signal, being measurements restricted to round-trip delays shorter than the signal's period. The round-trip delay between the emitted and the received signal causes a constant frequency difference, $f_d$, which is directly proportional to the distance to the target (Fig. 4c). The frequency difference is obtained by a coherent detector that mixes the return signal with the local oscillator (LO). This approach presents several advantages such as: (1) the LO allows for a higher system gain, achieving higher SNR values [25]; (2) the phase and frequency coherence of the received light and the LO provides higher robustness to sunlight and other external light sources interference [37]; (3) it makes possible to directly measure the targets' velocity due to the Doppler shift presented in the return signal [38]; and (4) since it operates in continuous-wave, it avoids high peak power emissions that can cause eye safety issues.

The biggest challenge of this architecture is the significant increase in laser/optical requirements [28]. The laser must keep phase integrity for enough time to be able to measure distances without a meaningful error. The longer it keeps the integrity, the longer distances can be measured, since even small phase variation during the process impacts the system SNR. This increases the system's complexity, making it expensive to create laser solutions that must narrow in terms of spectrum, but tunable in terms of frequency. Moreover, and regarding the optical system, it is crucial to synchronize the LO with the returning signal to achieve the best SNR.

## V. LiDAR Imaging Systems

There are several imaging architectures that can be used to recreate the surroundings of a vehicle [31], [39], which

implement the measuring methods previously discussed [30], [32]. Typically, LiDAR systems can be categorized in: (1) beam steering sensors that use a rotor-based mechanical part to scan the entire environment [26], [40]; (2) solid-state beam steering sensors without requiring bulky spinning mechanical components [41]–[50]; and (3) full solid-state sensors with no mechanical moving parts [51]–[54].

### A. *Rotor-Based Mechanical LiDAR*

Rotor-based mechanical LiDAR sensors are the most mature imaging technique being used by the automotive industry [26], [40]. Widely used in driverless systems, they can provide a 360° horizontal FoV, with different vertical FoV ranges. For instance, Waymo, the Google's self-driving car project that became an independent company in 2016, operates a commercial self-driving taxi service running across different USA states with a rotor-based mechanical LiDAR on top of the vehicle. The 3D 360° horizontal FoV is achieved through a mechanical rotation system that spins the scanning part. Vertically, the FoV is defined by the number of existing emitter/receptor pairs, also known as channels. Despite its broad utilization, this type of sensor presents several disadvantages, such as the bulky rotating part and the inertia it adds to the system, the overall power consumption, and weight. Considering the recent trends and technologies for LiDAR sensors, rotor-based systems are considerably more expensive. Among Velodyne, the company that has pioneered this technology, Hesai, Ouster, Quanergy, and Robosense, also provide rotor-based mechanical LiDAR sensors.

### B. *Scanning Solid-State LiDAR*

Solid-state LiDAR systems have no spinning mechanical parts and present reduced FoV, which usually makes them cheaper. However, several automotive solutions combine multiple sensor outputs with the vehicle's surroundings to recreate a wider FoV. This type of LiDAR imaging system is bringing new technologies to the LiDAR arena, such as Microelectromechanical (MEMS) [41]–[45], and optical phased array (OPA) systems [46]–[50].

***Mirror MEMS*** solutions include MEMS technology to deploy tiny electromechanical mirrors to replace the external rotating parts. Rather than mechanically moving the laser position across the FoV, this approach uses a static laser that points to electromechanical mirrors that can change their tilt angle by applying a pull-in voltage. However, the moving nature of a vehicle can affect the performance of such systems since they are constantly subject to vibrations and shocks. MEMS mirrors can be classified into resonant and non-resonant [41]. Resonant mirrors can achieve larger scanning angles at high frequency by using simple control algorithms. The downside of this solution is the sinusoidal scanning trajectory, which leads to unstable scanning speeds. In contrast, non-resonant mirrors can provide more freedom on the scanning path (it can follow a triangular or saw tooth trajectory) [42], however, it requires a sophisticated controller to keep the scanning performance during scanning trajectories at a constant speed [43]. Since they provide a low scanning range, they require additional optics and lens systems [44].

To achieve 3D scanning capabilities, 2D MEMS laser projectors are implemented based either on a single mirror with two oscillation axes or using two different mirrors, one for each axis. While the latter provides more robustness to vibrations and it is easier to fabricate due to its straightforward design, the former provides advantages in packaging and axis alignment, resulting in a sensor with better accuracy. One of the most common system architectures in MEMS LiDAR sensors is raster scanning [45]. It deploys one mirror in a low frequency non-resonant mode to determine the system frame-rate, and one high-frequency resonant mirror covering the other axis. Since the angular resolution is the result of the ratio between the two frequencies, it can be tuned solely by changing the non-resonant frequency.

In automotive applications, the faster mirror, usually responsible for the horizontal axis, presents frequencies between 0.5 and 2kHz, while the slower mirror, responsible for the vertical axis, operates at frequencies between 10 to 30Hz. Alongside the reduced FoV that ranges from 25° to 150°, MEMS-based systems also present limitations in terms of range comparing with mechanical rotor-based sensors, since the emitted power needs to be reduced to avoid damaging the sensible parts of the MEMS mirror. Examples of manufacturers that offer MEMS-based LiDAR sensors are Blickfeld, Innoviz, RoboSense, and ZVISION.

***Optical phased array (OPA)*** systems, similarly to a phased array Radar, employ phase modulators to optically steer the laser beam. By controlling the departure/arrival time of the beam that travels through the lens, the modulator can change the signal's shape [46]. The result is a direction-controlled emitting light, that can be achieved by applying different phases into an array of laser emitters (Fig. 5). The receiver controls the receiving light in the same way, which allows the sensor to collect only light from the spot that is being illuminated, eliminating unwanted signals from other sources and reducing the multi-path reflection phenomena [47], [48]. Because OPA-based approaches do not employ any moving part, there is an on-growing interest in this technology [49], [50]. Not only it can be fully integrated on a chip, but due to the lack of inertia, it can potentially achieve faster scanning rates (100kHz) when compared with other mechanical solutions. However, due to the inherent laser power loss, LiDAR sensors based on this technology are currently being deployed in short- and mid-range solutions. Examples of manufacturers that deploy LiDAR systems with OPA technology are Quanergy and Robosense.

### C. *Full Solid-State LiDAR*

Flash LiDAR systems are considered solid-state due to the lack of mechanical rotating parts. Their operation is very similar to standard digital Cameras, which use a flash light to illuminate the entire environment while photodetectors collect the back-scattered light [51], [52]. Since all FoV points simultaneously share the light source, it not only allows faster data capture but can also be highly immune to light distortion [53].

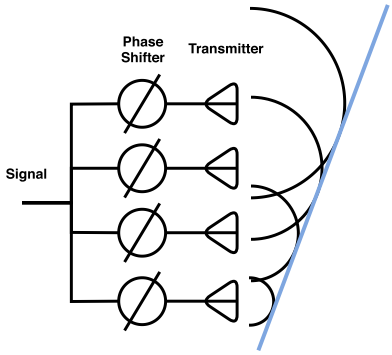


Fig. 5. Optical phase array principle.

However, the receiver must be able to differentiate the returning light from each point. Flash LiDAR sensors are generally implemented with photodetector arrays, whose density defines the sensor spatial resolution, turning them into an expensive solution [54]. When compared with other scanning techniques, the flash LiDAR emitter requires more power to illuminate the entire FoV. Thus, the maximum detection range is limited (between 50 to 100m), which reduces their application to blind-spot detection of large objects such as cars and pedestrians. In general, these sensors tend to be more straightforward in terms of the mechanical and optical systems, but usually require more sophisticated electronic components [28]. Examples of manufacturers that offer flash-based LiDAR sensors are ASC, LeddarTech, Ouster, Sense Photonics, and Xenomatics.

### *D. Emerging Technologies and Hybrid LiDAR Systems*

Despite mechanical rotors, solid-state, and flash being the most common approaches among commercial scanning LiDAR sensors, some manufacturers present other interesting approaches in their imaging techniques.

***Liquid-immersed polygon LiDAR*** by Mirada Technologies presents a novel rotating mirror approach by immersing the rotating unit into a fluid. Fluid stabilization can solve not only automotive shock and vibration problems, but also heat and lubrication issues.

***VCSEL*** is a type of semiconductor laser diode that, contrarily to conventional edge-emitting semiconductor lasers, emits light perpendicularly to the active region. Although this technology had its first developments between 1965 and 1990, it is still used in multiple modern light applications such as optical fiber data transmission or laser cutting machines [55]. Due to features such as on-wafer testing (it promotes the manufacturing of cheaper products), low power consumption, and circular light beam output, several manufacturers started to integrate this technology into their LiDAR sensors [56]. Examples of manufacturers that use VCSEL in their products are Trilumina and Sense Photonics.

***Spectrum-Scan*** technology, by Baraja, applies the laser light into a prism-shaped material rather than using rotating lasers or moving mirrors, which allows scanning different angles instantaneously. Moreover, a prism allows changing the laser wavelength and color, providing extreme adaptability features. In addition, by employing just one laser in their multi-sensor setups, the company claims to achieve a true interference immunity between other LiDAR sensors.

***Micro Motion Technology (MMT)*** is patented by Cepron and differs from traditional beam-steering technologies by deploying a mirrorless, frictionless, and rotation-free LiDAR system. Such technology increases the product's reliability and manufacturability while delivering high performance and low power at an affordable price. More details about this technology are not yet disclosed.

***Hybrid solutions*** that combine different imaging techniques are also being explored. However, due to the companies being continuously disputing for a market spot, most of the product's details are undisclosed. LeddarTech, one of the strongest players in solid-state LiDAR solutions, presents the concept of hybrid flash solid-state LiDAR. By combining the flash principle with a receptor based on MEMS beam steering and high-performance photodetectors, they claim that the result is not only a cost-effective product but also a robust and reliable sensor. Velodyne is also creating solid-state hybrid (SSH) systems, where solid-state mechanisms are being added to the mechanical spinning parts.

## VI. On-Chip Solutions and Commercial LiDAR Sensors

Manufacturers often strive to create solutions under the SWaP-C premises, which stand for size, weight, power, and cost. With this in mind, compacting LiDAR sensors into on-chip solutions can be a significant breakthrough in the automotive arena. For instance, SilC is making the first steps towards on-chip solutions by developing an on-chip FMCW LiDAR. Their platform offers a cost-effective solution by integrating all the high-performance components into a single small silicon chip through mature semiconductor processes, allowing big-scale manufacturing of low-cost and low-power sensors. Small sensors can provide flexible arrangements with a strategic sprinkled distribution around the car.

LeddarTech, a company founded in 2007 and used to provide LiDAR solutions for autonomous driving, offers on-chip solutions based on the LeddarEngine platform [57]. The platform consists of a system-on-chip with dedicated digital signal processors, data acquisition modules, and management software (LeddarSP), allowing, customers to enhance customized LiDAR solutions with specific requirements to support autonomous driving features.

Nowadays, there is a broad number of commercial LiDAR solutions available in the market. Even if the scope is reduced only to commercial products applied to automotive, there are already several players with different products that deploy different ToF measurement and imaging techniques, already discussed in the previous sections. Table I presents state-of-art LiDAR systems provided by the biggest and prominent players in the market, summarizing them in terms of their imaging technology, range, scanning rate, horizontal and vertical FoV, resolution, point rate, and laser's wavelength. Some information is not yet available (n/a) since manufacturers sometimes protect several product details.

TABLE I
STATE-OF-THE-ART LiDAR SENSORS AVAILABLE IN THE MARKET

| ***Manufacturer** (model)* | ***Type*** | ***Range*** | ***Scan R.*** | ***FoV** (V×H)* | ***Res.** (V×H)* | ***Point R.*** | ***Wavelength*** |
|---|---|---|---|---|---|---|---|
| AEye 4Sight M | Solid-State MOEMS | 1000 m | 100 Hz | 30º x 60º | 0.1º x 0.1º | 4M p/s | 1550 nm |
| Aurora (Blackmore AFDL) | Doppler LiDAR | 450 m | n/a | 30º x 120º | 0.1º x 0.1º | 2.4M p/s | 1550 nm |
| ASC Peregrine | 3D Flash | 75-5500 m | 30 Hz | 15º x 60º | 0.47º x 0.47º | 82K p/s | 1570 nm |
| ASC Tigercub | 3D Flash | 200-9000 m | 30 Hz | 60º x 60º | 0.47º x 0.47º | 328K p/s | 1570 nm |
| ASC Goldeneye | 3D Flash | 200-5000 m | 20 Hz | 60º x 60º | 0.47º x 0.47º | 328K p/s | 1570 nm |
| Baraja Spectrum-Scan | RMCW | 200 m | n/a | n/a | n/a | n/a | 1550 nm |
| Blickfeld Cube 1 | MEMS Mirrors | 250 m | 10 Hz | 30º x 70º | 0.4º x 0.4º | 2M p/s | 1550 nm |
| Blickfeld Cube Range 1 | MEMS Mirrors | 250 m | 10 Hz | 12º x 18º | 0.24º x 0.24º | 2M p/s | 1550 nm |
| Cepton Vista-P90 | MMT | 200 m | 20 Hz | 40º x 90º | 0.38º x 0.13º | 312K p/s | 905 nm |
| Cepton Vista-X120 | MMT | 200 m | 40 Hz | 20º x 120º | 0.13º x 0.13º | n/a | 905 nm |
| Cepton Sora-P90 | MMT | 200 m | 380 Hz | 40º x 90º | 0.08º x 0.35º | n/a | 905 nm |
| Hesai Pandar40P | Mechanical rotor | 200 m | 20 Hz | 40º x 360º | 0.33º x 0.4º | 720K p/s | 905 nm |
| Hesai PandarQT | Mechanical rotor | 30 m | 10 Hz | 104.2º x 360º | 1.45º x 0.6º | 384K p/s | 905 nm |
| Hesai PandarGT | 2D Solid-State | 300 m | 20 Hz | 20º x 60º | 0.07º x 0.1º | 945K p/s | 905 nm |
| Hybrid Lidar Systems Lissa | 3D Flash | 200 m | n/a | 40º x 120º | n/a | n/a | n/a |
| Innoviz InnovizPro | MEMS | 600 m | 20 Hz | 20º x 73º | 0.45º x 0.2º | 7.5M p/s | 905 nm |
| Innoviz InnovizOne | MEMS | 250 m | 20 Hz | 25º x 115º | 0.1º x 0.1º | 7.5M p/s | 905 nm |
| Innovusion Falcon | Solid-state | 280 m | 10 Hz | 30º x 110º | 0.13º x 0.14º | 6.5M p/s | n/a nm |
| LeddarTech Pixell | 3D Flash | 40 m | 20 Hz | 16º x 177.5º | 2º x 1.9º | n/a | 905 nm |
| Livox Horizon | Solid-state | 280 m | n/a | 25.1º x 81.7º | 0.13º x 0.14º | 240K p/s | 905 nm |
| Luminar Hydra | Non-Rotating Mechanical, Flash | 250 m | 30 Hz | 30º x 120º | 0.03º x 0.07º | n/a | 1550 nm |
| Mirada | Polygon Laser, Air Immersion | n/a | n/a | n/a | n/a | n/a | n/a |
| Ouster OS-0-128 | Mechanical rotor | 55 m | 20 Hz | 95º x 360º | 0.7º x 0.18º | 2.6M p/s | 850 nm |
| Ouster OS-1-128 | Mechanical rotor | 105 m | 20 Hz | 45º x 360º | 0.35º x 0.18º | 2.6M p/s | 850 nm |
| Ouster OS-2-128 | Mechanical rotor | 240 m | 20 Hz | 22.5º x 360º | 0.18º x 0.18º | 2.6M p/s | 850 nm |
| Phantom Intelligence Sentinel | 3D Flash, DSP | 35-200 m | n/a | 25º x 3.9º | n/a | n/a | 905 nm |
| Phantom Intelligence Guardian | 3D Flash, DSP | 40 m | n/a | 25º x 1.5º | n/a | n/a | 905 nm |
| Quanergy M8 | Mechanical rotor | 200 m | 20 Hz | 20º x 360º | 0.2º x 0.2º | 420K p/s | 905 nm |
| Quanergy S3 | OPA | 200 m | 25 Hz | 4º x 50º | 0.5º x 0.5º | n/a | 905 nm |
| RoboSense RS-LiDAR M1 | MEMS Solid-state | 150 m | 20 Hz | 25º x 120º | 0.2º x 0.2º | 1.1M p/s | 905 nm |
| Sense Photonics Osprey 30 | Solid-State VCSEL, 3D Flash | 15-25 m | n/a | 80º x 30º | 0.27º x 0.27º | 330K p/s | 940 nm |
| Sense Photonics Osprey 75 | Solid-State VCSEL, 3D Flash | 10-15 m | n/a | 80º x 75º | 0.27º x 0.27º | 820K p/s | 940 nm |
| SiLC 4D+ Vision Chip | FMCW, On-Chip | n/a | n/a | custom | custom | custom | 1550 nm |
| Velodyne VLP-16 | Mechanical rotor | 100 m | 20 Hz | 30º x 360º | 2º x 0.4º | 289K p/s | 903 nm |
| Velodyne HDL-64E | Mechanical rotor | 120 m | 20 Hz | 27º x 360º | 0.4º x 0.35º | 1.3M p/s | 903 nm |
| Velodyne VLS-128 | Mechanical rotor | 300 m | 20 Hz | 40º x 360º | 0.11º x 0.4º | 8M p/s | 903 nm |
| XenoLidar Highway | 3D Flash | 200 m | 20 Hz | 10º x 30º | 0.2º x 0.2º | n/a | 905 nm |
| XenoLidar Intercity | 3D Flash | 50 m | 20 Hz | 20º x 60º | 0.3º x 0.3º | 270K p/s | 905 nm |
| ZVISION ML-30 | FMCW, MEMS | 30-85 m | n/a | 30º x 120º | 0.1º x 0.3º | n/a | n/a |
| ZVISION ML-80 | FMCW, MEMS | 80-220 m | n/a | 30º x 120º | 0.1º x 0.3º | n/a | n/a |
| ZVISION ML-X | FMCW, MEMS | 200 m | n/a | 20º x 60º | 0.2º x 0.3º | n/a | n/a |

## VII. DEVELOPMENT PLATFORMS AND SIMULATORS

The increased interest in autonomous driving turned LiDAR solutions into a hot topic. As a result, not only new commercial LiDAR sensors emerged, but also development boards and simulators that can be used to speed up the development, debug, and testing phases.

***AD-FMCLIDAR1-EBZ*** is the first LiDAR prototyping platform, released by Analog Devices in 2019 [58]. Due to its modular approach, it can be used not only for developing algorithms for a specific LiDAR subsystem (e.g., data acquisition and signal transmission), but also for testing different techniques that can be adopted in a broad range of applications. The platform is composed of three different boards: ***(1) Data Acquisition Board (DAQ)***, which is responsible for acquiring data at high speeds and control the system clock. Since there is an FMC connector interface, developers can plug different FPGA boards to test their algorithms. There are two more modules connected to the DAQ board by digital FMC interfaces: a ***(2) Laser Transmitter Board***, which includes four distinct lasers with a proper precision driver and power needed for firing the lasers; and the ***(3) AFE Receiver Board***, which is equipped with several sensors (16 channel APD from First Sensor and four ADI LTC6561 Quad-channel TIA's). This board provides the optics required to receive data, allowing also custom optics to be added.

***Auto and Mobility LiDAR Platform*** from Leddartech is composed of the LeedarEngine SoC [57], DSPs, plug-and-play optics, sensors, software, and ADAS services. This ecosystem, tailored for industry development, allows fast prototyping and validation before releasing final products into the market. Due to its commercial nature, this platform is mainly available for industrial development.

***AEye iDAR*** is an artificial perception platform designed to integrate new technologies and algorithms into Camera/LiDAR setup combinations [59]. Their most recent product, the 4Sight sensor, combines a Camera and a LiDAR empowered by the iDAR platform. It provides not only $60° \times 30°$ FoV with resolutions of $0.1°$ up to 100 Hz frame rate and more than 200 meters of range, but also presents colored point clouds, regions of interest, and perception and classification definable software designed for automotive applications.

***Apollo open autonomous driving platform*** is an open-source architecture that offers multiple core modules for autonomous driving, accelerating the development, testing, and deployment of autonomous solutions [60]. On its most recent version, besides all of the low-level software components to control the vehicle, it also offers modular cores for localization, perception, predictions, planning, cloud services, simulation, Vehicle-to-Everything, and DuerOS for telematics products. In addition, it supports most of the current sensors used in the automotive industry, allowing a straightforward deployment of autonomous solutions.

***rFpro and AAI Sensor Simulation*** are two simulators widely used by the automotive industry that are able to emulate several LiDAR sensors and generate data outputs that can be used to test and validate Supervised Learning systems for ADAS and Autonomous applications [61], [62]. LiDAR applications require different setups and sensor characteristics, for which simulation tools can help in mitigating the hard task of testing new techniques, e.g., imaging or measuring, in different scenarios at extreme environmental conditions. The success of using Deep Neural Networks (DNNs) on object detection and classification mechanisms in LiDAR applications [63] has triggered the need for simulators and dataset generators. Because DNNs require a huge amount of data for the training phase, using data directly from the real sensor can be a hard task [64]. Moreover, and since weather can cause interference on the perception systems [65], rFpro can also emulate weather conditions, shadows, and light interference, providing accurate datasets close to the real world and mitigating the hard task of creating huge laboratory setups.

## VIII. LiDAR Challenges

Despite LiDAR sensors being widely adopted by the automotive industry towards autonomous driving vehicles, this technology still faces several challenges. Besides the measuring and imaging technology previously discussed in sections IV and V, the car industry, technology companies, and academia, keep putting efforts into performing research on important topics such as sensor calibration, data compression, mutual interference, image filtering, and object detection and classification mechanisms. Table II summarizes current challenges and state-of-the-art solutions to mitigate them.

### *A. Sensor Calibration*

LiDAR sensors require different calibration steps before they can be efficiently used by the perception system of the car, which can either be intrinsic or extrinsic. Intrinsic calibrations are used to eliminate the uncertainties (errors) caused by tolerances in LiDAR components and the manufacturing process, e.g., the output from micro-mechanical mirrors or the wrong placement of the laser. Such calibrations can be managed during the manufacturing process at end-of-line testing, or by later adjusting the sensor's output when pointed to well-known targets in a controlled environment. Several intrinsic calibration methods based on planar surfaces have been applied to automotive LiDAR sensors, which consist of using structures with known geometry and shapes, e.g., polygonal rectangular/triangular boards and spheres, that can also include 2D patterns [66]–[70]. The Velodyne HDL-64E sensor is being a good case study on how intrinsic calibrations can improve the overall point cloud output in terms of accuracy and precision [66], [69]. However, such calibrations often require special tuning on sensor components and output.

Extrinsic calibrations are used to improve the intrinsic parameters of the LiDAR or to tune the perception system of the car by combining distinct sensor outputs under different setups, which may include LiDAR sensors [71]–[73], LiDAR and Cameras [74]–[80], and LiDAR with GPS/IMU sensors [81], with or without well-known targets. Setups that combine both LiDAR and Cameras propose calibration methods based on the observation of static targets [75], [76]. Despite such calibrations being performed in controlled environments, further real-world experiments proved the reliability of these methods. However, they can only be performed when calibration targets are available, and sometimes requiring complex setups, hampering the re-calibration after the sensor's deployment. Target-less calibrations using the combination of LiDAR and Cameras have also been proposed [77], [80]. Despite presenting benefits in terms of dynamic on-the-fly calibrations without requiring artificial targets or structured environments, they still require improvements to compete with target-based methods.

### *B. Mutual Interference*

LiDAR sensors are expected to have large-scale adoption in the very near future, being a key instrument on the perception system of a car. However, the imminent probability of mutual interference between sensors becomes an important issue, where surrounding signals may cause reduced SNR and ghost target problems. Despite some measuring principles and imaging techniques being more robust and immune to noise, it is necessary to ensure the uniqueness of the signals emitted by each sensor. Several studies have shown the big challenge of avoiding mutual interference between LiDAR, considering both spatial and temporal overlaps [82]–[85].

Current mitigation methods for FMCW-based systems propose the utilization of specific signal formats with modulation coding techniques [85]. To achieve signal orthogonality, several approaches were designed based either on code division-multiple-access (CDMA) [34], pseudo-random bits modulation, and true-random bits modulation. Since CDMA-based approaches present limitations when it is required to assign orthogonal codes for a significant number of sensors, implementing these solutions on applications such as autonomous vehicles becomes a hard task. On the other hand, random-based approaches require bit generators at very

high frequency in order to support high scanning rates with low latency in target detection. Due to the efficiency of analog true-random signals on Radar sensors, some approaches with the same concept were also applied to LiDAR [86]. However, these methods may require extra optical hardware with a high-speed modulation capacity.

A true-random LiDAR solution has also been proposed [87]. It uses an analog true-random signal generator for the transmitted signal and an optical coherent detector for the receiver. The obtained results have proved the mutual interference immunity regardless of the signal formats of the interference sources, where different scanning techniques were used, e.g., continuous-wave, pulsed light, and FMCW. Despite being an extremely important topic, mutual interference immunity in LiDAR sensors is quite challenging and still at an early stage of development. Thus, further solutions must be proposed as LiDAR sensors will soon become mainstream.

### *C. Data Compression*

Modern LiDAR sensors already support higher resolutions and wider field of view (FoV) capabilities, which help in creating better 3D representations of the surroundings. However, the real-time point-cloud data output that has to be processed can reach several Gbit/s. For instance, the Velodyne VLS-128 can produce up to 9.6M points/second. Data handling, storage, and transmission are some of the most challenging aspects of a LiDAR system [88]–[90]. While some solutions try to mitigate this problem during data acquisition [88], others focus on compressing data after being captured and transferred to a computing unit [90], [91].

LASzip [92], LAScompression [93], and real-time point cloud compression [89], [94], [95] propose compression over 3D LiDAR point clouds. While LASzip and LAScompression add lossless compression over the standard LAS format, the work presented in [94] proposes the decomposition of 3D data into a 2D matrix, allowing a faster compression method. By its turn, the solution presented in [95] uses a deep-learning approach to detect and compress redundant data, allowing real-time processing and outperforming other tree-based approaches [96]. Moreover, the Moving Picture Experts Group (MPEG) has been working on the development of the geometry-based point cloud compression (G-PCC) standard [89], which addresses the compression of point clouds in both Category 1 (static point clouds) and Category 3 (dynamically acquired point clouds).

Furthermore, conventional image compression methods were being used to solve data size problems [97], [98], showing its applicability in better data storage and efficient transmission to high-level applications. Nonetheless, performing the compression tasks adds significant processing overhead, which can be accepted for storage purposes, but may heavily penalize real-time applications that rely on the sensor's output.

### *D. Weather Denoising*

LiDAR sensors can be very sensitive to adverse weather conditions, such as fog [99], rain [65], and snow [100], which can severely affect the 3D point cloud [99], [101]. Many approaches have been proposed to mitigate this problem such as ROR/DROR [100], SOR/FCSOR [102], and LIOR [103].

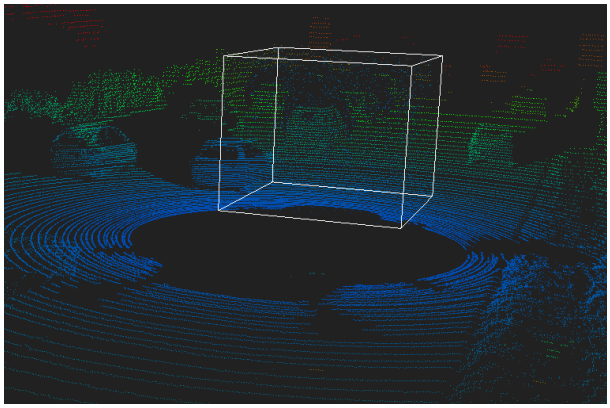

Fig. 6. Point cloud noise caused by heavy snow fall.

***Radius outlier removal (ROR)*** consists of a simple technique that computes the distance of each point to its neighbors, within a specific search radius, on a k-d tree data structure. When the number of neighbor points is below the defined threshold, the point is classified as an outlier. Despite being very easy to implement, the ROR algorithm does not perform well for distant objects in 3D LiDAR point clouds due to variations in the point distances. Thus, distant points are often wrongly classified as outliers. To address this limitation, the dynamic radius outlier removal (DROR), rather than using static search, changes the radius value as the distance to the measured points increases [100]. In tests with falling snow, the filtered point clouds presented improvements over 90%, outperforming convectional outlier removal filters. However, applying such filtering techniques can be quite slow, limiting the DROR utilization in real-time applications.

***Statistical outlier removal (SOR)*** is a denoising method that, similarly to ROR, removes the outlier points based on neighbors' information. However, instead of using a fixed radius and a minimum threshold for the number of neighbors, it calculates first the average distance of each point to its neighbors, defined as "k-nearest neighbor", rejecting the points which distance is higher than the average value plus the standard deviation. Despite improving ROR in detecting outliers, SOR severely increases the computation overhead. For this reason, Balta *et al.* have proposed the fast cluster statistical outlier removal (FCSOR) [102]. Before calculating the distance to neighbors, FCSOR performs a sub-sampling of the point cloud with a voxel grid filter step (all points inside a predefined 3D box are down-sampled to an approximated center point). However, and despite the computation complexity being decreased due to the number of clusters being reduced, it still does not provide real-time and the success rate in detecting outlier points slightly decreases. Fig. 6 depicts the SOR algorithm applied to a point cloud retrieved with the vehicle under heavy snowfall. The area inside the cube shows the detected points that are going to be removed by the algorithm.

***Low-intensity outlier removal (LIOR)*** is a method proposed by Park *et al.* that removes the noise caused by snow or rain

by using the intensity values of the reflected light [103]. Noise points usually present a lower intensity value when compared with neighbors at the same range, thus, every point below a defined threshold value is considered an outlier point. To reduce the false positive ratio, a second step is also applied to an outlier, which can be turned into an inlier if several neighbors (defined by a threshold number) are detected within a specified distance to this point. When comparing LIOR with the previous filtering methods, it can achieve filtering speeds up to twelve times faster than SOR, and eight times faster than the DROR. However, real-time filtering in high-speed vehicles is only possible if the method is applied only to certain regions of interest rather than the whole point cloud. Regarding the filtering accuracy, the noise points can be filtered with the same efficiency as the DROR method. However, LIOR can achieve a false positive ratio of 1%, while DROR can reach almost 50% of points wrongly classified as outliers.

***WeatherNet*** is the first convolutional neural network (CNN)-based approach applied to LiDAR point clouds that aims to understand the underlying data structure of weather-related noise [104]. To boost the computation speed, this approach uses 2D projections of the point cloud to feed the CNN, achieving great results both in filtering accuracy and filtering speed. Due to the lack of point cloud data retrieved in real-world situations with adverse weather conditions, the learning process of this method can still be a challenge. To help in filling this gap, WeatherNet uses a data augmentation approach to add realistic weather effects to point cloud data, gathered in a controlled environment with a climatic chamber. However, since fog and rain models were used to manipulate and create bigger data sets, further tests are required to evaluate the solution in real-world scenarios.

### *E. Ground Segmentation*

Ground segmentation is an important processing step that aims at detecting the road surface by identifying and separating the ground points from a point cloud, helping in reducing the complexity and performance of the subsequent tasks. Existing ground segmentation approaches can be divided in elevation maps [105], [106], ground modeling [107]–[110], adjacent points [111]–[114], Markov random field (MRF)-based methods [115]–[120], and learning-based methods [121]–[123]. Despite this broad range of solutions, some of them still face several problems in balancing accuracy (over- and under-segmentation) and the computational requirements (slow-segmentation), which can highly affect the overall performance of the vehicle's perception systems [120], [124].

***Elevation map*** methods are straightforward approaches that consist in structuring the 3D point cloud into a 2.5D projection (grid model), i.e., a horizontal plane with an elevation map [105], [106]. Next, for each cell of the grid, the algorithm calculates the average height values of the points within the cell. Based on a defined threshold, a point can be classified as ground or non-ground. Segmentation algorithms based on elevation maps assume the presence of ground points in the grid and that the grid is flat, which can cause under-segmentation problems when the ground is sloped with vegetation, hills, or curbs. Solving this problem would require setting a larger classification threshold. However, increasing such threshold can then lead to serious over-segmentation issues.

***Ground modeling*** methods also use a grid map to model the ground and extract non-ground points. For instance, Himmelsbach *et al.* proposed 2D line extraction algorithms applied to every cell on a polar grid map. Next, every point is compared with each ground plane line in order to classify the ground from non-ground points [107]. To create the ground segmentation, Chen *et al.* have used 2D Gaussian Process Regression (GPR) with sparse covariance functions over a circular polar grid map created from the 3D point clouds [108]. Because the large-scale 2D ground segmentation requires many calculations, in further research, authors have suggested a new approach that splits the problem into many simple GPR problems with lower complexity [109]. Despite achieving real-time with fair ground classification results, the algorithm is insensitive to slowly rising obstacles such as stair steps. More recently, Kaiqi et. al have combined GPR with the robust locally weighted regression (RLWR) algorithm [110]. The solution consists in dividing the point clouds that are projected on the circular polar grid map into radial and circumferential filtering processes to form a hybrid regression model, which can eliminate outlier points and model the ground surface in a more robust way. Despite achieving good results for ground detection, even with sparse point clouds or uneven grounds, the required computational time does not fit with the real-time requirements of an automotive LiDAR.

***Adjacent points*** methods address the ground segmentation problem by using neighborhood relationships between points in the 3D point cloud, which are used to extract local features from the normal vectors of estimated points. For instance, some methods use an optimal hierarchical clustering approach to unorganized point clouds based on a proximity matrix composed of a distance and a direction term. The dissimilarity calculation of two clusters is based on the Euclidean distance between a pair of points selected from each cluster [111], [112]. In further research, the authors proposed a pipeline of the accurate plane segmentation for point clouds to address the shortcoming in the local optimization [113]. In the evaluation of two datasets, this method has shown better correctness and completeness results. However, and despite outperforming other segmentation algorithms, the complexity of these solutions fails in providing the real-time requirements of an autonomous driving scenario. With the real-time requirements in mind, the work from Serafin *et al.* proposes a feature-based approach using Principal Components Analysis (PCA) of neighborhoods of points, which results in mathematically principled line and plane features [114]. Despite providing a fast method, it only provides good results with flat regions.

***Markov random field (MRF)-based*** methods have been widely used in ground segmentation tasks. For instance, Ruso *et al.* have proposed a new approach for labeling 3D points with different geometric surface primitives using a novel

feature descriptor and discriminative graphical models [115]. By defining classes of 3D geometric surfaces and making use of contextual information using Conditional Random Fields (CRF), the system successfully segments and labels 3D point clouds based on the type of surfaces the points are lying on. Lukas *et al.* presented an adaptative method based on a local ground elevation estimation to model the ground as a Spatio-Temporal CRF (STCRF) [116]. The CRF algorithm is used to unify the spatial and temporal dependencies within the segmentation process, while an Expectation Maximization (EM) algorithm estimates in parallel in each node the ground elevation parameters. One of the advantages of these methods is the successful segmentation of ground points in several environments with near-real-time performance. Guo *et al.* [117] and Byun *et al.* [118] describe the gradient cues of the road geometry to construct an MRF. By using a belief propagation (BP) algorithm, they partition the surrounding environment into different regions, e.g., reachable, drivable, obstacles, and unknown. Because the results of these approaches are relatively coarse, Zhang *et al.* have proposed an improved method that uses a loopy BP (LBP) algorithm [119]. While this approach has shown good performance results in rough terrains when compared with the other methods, it still faces the problem of the required number of interactions to perform, which results in a non-real-time solution. Velas *et al.* [125] further improved the work by Zhang *et al.* [119] by using a new encoding method for the sparse 3D data points suitable for training a CNN. Furthermore, and motivated by previous research, Huang *et al.* have recently proposed a fast point cloud ground segmentation approach based on a coarse-to-fine MRF method [120]. This method can highly reduce the computational complexity while improving both the accuracy and real-time aspects with a better environmental adaptability.

***Learn-based*** methods have been widely used by camera-based systems in ground segmentation tasks, achieving impressive results especially with deep learning techniques [126], [127]. However, camera-based systems alone cannot guarantee the reliability of such methods due to dynamic lighting conditions in outdoor environments. Regarding deep learning methods applied to 3D point clouds, Landrieu *et al.* have proposed a novel framework to tackle the challenge of semantic segmentation of large-scale point clouds captured by a superpoint graph (SPG) structure [121]. The SPG is then exploited by a graph convolutional network to complete the ground segmentation task. Motivated by the low training speeds and complex network architectures of other deep learning methods, Zhang *et al.* introduced ShelNet [122], an efficient neural network based on a simple convolution operator that uses concentric spherical shells to represent the point sets. By their turn, Hu *et al.* presented RandLA-Net, an efficient and lightweight neural architecture that uses random point sampling (instead of complex point selection approaches) to directly infer per-point semantics for large-scale point clouds [123]. Despite achieving efficient results and good training speeds, both approaches still face the problem of covering a wide range of ground scenarios in an automotive application.

### *F. Simultaneous Localization and Mapping (SLAM)*

Simultaneous Localization and Mapping (SLAM) has been widely used in robots for building real-time localization maps solely based on their perception sensor data and odometry algorithms. A lot of research has been made to propose the utilization of SLAM with autonomous vehicles, where the main challenges rely on providing real-time mapping while dealing with the 3D point cloud data. Odometry systems can rely on data from sensors such as IMUs, Cameras, LiDAR, etc., which can be sometimes combined to improve the accuracy and convergence speed.

Several LiDAR-only SLAM methods have been proposed. For instance, LOAM is considered the current state-of-the-art SLAM algorithm that uses only LiDAR odometry for a real-time mapping using ranging measurements from a 2-axis LiDAR moving in 6-DOF [128]. The main idea is to divide the problem into two algorithms, where one estimates the LiDAR velocity by performing odometry at a high frequency but low fidelity, while the mapping algorithm runs at a lower frequency (called only once per sweep) for fine matching and point cloud registration. LOAM provides low-drift and low-computational complexity without requiring high accuracy ranging or IMU sensors. Other methods have followed LOAM. For instance, Deschaud [130] has proposed IMLS-SLAM, a new scan-to-model matching framework. First, the method performs a specific sampling strategy to create the unwarped point cloud data from the first scan, which is followed by the iterative closest point (ICP) scan matching strategy and the Implicit Moving Least Squares (IMLS) surface representation. Despite reducing the drift problem and outperforming LOAM, it does not provide real-time capabilities.

Agrawal *et al.* proposed PCE-SLAM [129], a real-time SLAM for intelligent vehicles that uses a two-step sweep-to-sweep motion estimation and sweep-to-map registration that compensates the distortion of the point cloud, estimates the vehicle's motion, and generates the world's 3D map. Despite presenting fast and accurate results, the algorithm's accuracy can be affected by dynamic objects in the scene moving at speeds greater than 25 mph. DL-SLAM, proposed by Li *et al.* [131], is based on a direct 2.5D heightmap that extends previous research, the Direct Lidar Odometry (DLO), with segmentation features. Despite being also a LiDAR-only SLAM system, it can outperform DLO and LOAM due to the loop closure and graph-based optimizations added to DLO.

Because LOAM relies only on a LiDAR sensor, further approaches such as LOL [132] and AV-SLAM [133] attempt to correct the accumulated drift problem with offline data or other sensors. LOL applies a place recognition method to detect geometric similarities between the real-time 3D point cloud and an offline map used to refine the position estimation whenever a good match between maps is detected. The proposed method was tested with several KITTI datasets, providing good results in terms of relocalization accuracy and the precision of the vehicle's trajectory while keeping the real-time features. By its turn, AV-SLAM proposes the VI-SLAM method, which is a combination of three SLAM algorithms that use a different subset of sensors such as

TABLE II
CHALLENGES AND SOLUTIONS IN AUTOMOTIVE LIDAR SENSORS

| *Challenge* | | *Solution* | *Major advantage* | *Major disadvantage* |
|---|---|---|---|---|
| **Calibration** | Faults in sensor components | Intrinsic plane-based calibrations [66]–[70] | Improvements in sensor's accuracy and precision | Require special sensor tuning capabilities |
| | Mounting and external disturbances | Extrinsic calibration with multiple LiDAR [71]–[73] | Straightforward fusion and calibration | Unusual setup on automotive applications, specially with overlapping FOVs |
| | | Extrinsic calibration with LiDAR-Camera [74]–[80] | Most common and mature setup in autonomous vehicles with extremely precise results | Best proven methods force target calibration with specific setups, not allowing re-calibrations |
| | | Extrinsic calibration with LiDAR-IMU/GPS [81] | Common sensors in autonomous applications that allow target-less calibration | IMU/GPS sensors accumulate error overtime |
| | | Extrinsic target-based [71,72,74]–[76] | Extremely precise results | Re-calibrations require a proper setup |
| | | Extrinsic target-less calibrations [73,77]–[81] | Allow on-the-fly (dynamic) re-calibrations | Worse results than target-based calibrations |
| **Mutual Interference** | SNR degradation and ghost targets | CDMA-based approaches [34,85] | Achieve orthogonality based on simple codes | Do not escalate well on massive numbers |
| | | Pseudo- and True-random bit modulation [86,87] | Perform well with RADAR sensors | Require extra optical hardware with a high-speed modulation capacity |
| **Compression** | Point-cloud size | LAS-based approaches [92,93] | Standard and mature compression format | Require extra pre-processing steps and do not provide real-time compression/decompression |
| | | Tree-based approaches [89,96] | Allow real-time lossless compression | Limited to frame-by-frame compression |
| | | Voxel-based approaches [94,95] | Allow real-time compression/decompression using deep-learning methods | Reduce the point-cloud resolution |
| | LiDAR data stream | General-purpose lossless compression [88,90,97,98] | Allow real-time compression and storage optimization on processing units | Further studies are required to test the efficiency on automotive applications |
| **Point-cloud denoising** | Noise from adverse weather conditions | ROR-based [100] | Dynamic range filtering with good accuracy results | Do not provide real-time filtering and present high filtering rate of non-noise points |
| | | SOR-based [102] | Fast filtering speed due to low-complexity computation requirements | Do not provide real-time filtering capabilities |
| | | LIOR [103] | Approach that uses also the intensity achieving good results | Not providing real-time filtering on high-speed autonomous driving |
| | | WeatherNet [104] | CNN-based approach with fast and accurate results | Lack of extensive real-world testing and labeled data for training phases |
| **Point-cloud ground segmentation** | Ground filtering | Elevation maps [105,106] | Straightforward and fast methods | Can suffer from under- or over-segmentation |
| | | Ground modeling [107]–[110] | Good results even with uneven grounds | Slow-segmentation [108,110]; insensitive to slowly rising obstacles such as stair steps [109] |
| | | Adjacent points [111]–[114] | Fast methods that can explore the 3D features of a point cloud [111,112] | Do not provide real-time [113]; Only performs good with flat regions [114] |
| | | Markov random field (MRF)-based [115]–[120,125] | MRF-based methods that can perform fast with near-real-time results [115,116,120] | Some methods require several iterations to complete [117]–[119] |
| | | Learning approaches [121]–[123] | Good training speed and efficient results [122,123] | Lack of extensive real-world testing and labeled data for training |
| **SLAM** | Localization and Mapping | LiDAR-only approaches [128]–[131] | Explore the 3D point cloud in real-time | Can suffer from accumulated drift problems |
| | | Sensor and data fusion [132,133] | Reduce drift problems; can provide real-time | Require more sensors and offline data |
| | | Learning approaches [134] | Provide centimeter-level accuracy | Require multiple driving datasets |
| **Object detection and segmentation** | Object Segmentation | Point-based learning approaches [135]–[137] | Fast methods with great results on indoor scenes | Limitations on gathering spatial relationships |
| | | Projection-based learning approaches [138,139] | Fast approaches due to 2D representations | 3D information lost in 2D projections |
| | | Volumetric-base learning approaches [140] | Uses all 3D spatial relationships of the point | 3D representations limits the frame-rate |
| | Object detection | Multi-stage object detection [141] | Mature concept with proven results | Approaches with limited frame-rate |
| | | Single-stage object detection [63,142,143] | Faster methods; some provide real-time [143] | Reduced accuracy |

IMU-only, gray-scale mono-cameras, and LiDAR. Moreover, VI-SLAM includes a novel acceleration-based gravity direction initialization (AGI) method for the VI-SLAM algorithm that rapidly estimates the gravity direction from an initial unknown pose of the ego-vehicle.

Recently, new methods based on learning approaches started to emerge. For instance, Lu *et al.* have proposed $L^3$-Net [134], a learning-based approach based on several DNN structures that helps in achieving centimeter-level localization accuracy. Firstly, by using a lightweight version of PointNet, the method extracts a fixed number of local feature descriptors considering density, geometric characteristics, and distribution. Then it applies CNNs to infer the localization offset based on the descriptors. In the final step, Recurrent Neural Networks (RNNs) are used to achieve temporal smoothness since the localization task is a sequential process.

### *G. Object Detection and Segmentation*

An autonomous vehicle requires an accurate perception system to detect the surrounding environment, where real-time object segmentation and detection tasks are some of the biggest challenges currently faced by autonomous driving applications. The first LiDAR-based approaches applied hand-crafted features and sliding windows methods for the object detection, and Support Vector Machine (SVM) classifiers for the object identification [144], [145]. However, with the adoption of machine learning in the perception systems, several object segmentation and detection methods, which are well detailed in [146]–[148], can use deep learning for processing the 3D point cloud.

Methods based on semantic segmentation can be classified by the point cloud structure they use: (1) point-based [135]–[137]; (2) projection-based [138], [139]; and (3) volumetric-based [140]. PointNet [135] applies symmetrical operators to deal with raw (unordered) point clouds. Since they generate permutation-invariant feature extractors, the ability to capture spatial relationships between features is limited. To solve this problem, PointNet++ [136] proposes a hierarchical NN that applies PointNet recursively on a nested partitioning of the input point set. Despite being successfully evaluated in indoor scenes, these approaches present limitations when used in large-scale outdoor scenarios. Shi *et al.* proposed PointRCNN [137], a two-stage method to deal with 3D unordered point clouds. The stage-1 is used for the bottom-up 3D proposal generation, and stage-2 for refining proposals in the canonical coordinates to obtain the final detection results.

Regarding the projected grid-based structures (2D CNN segmentation), SqueezeSeg [138] uses a spherical projection of the point cloud to enable the usage of 2D convolutions alongside a CRF step to smooth the results. Due to the lack

of available datasets, SqueezeSeg deployed a LiDAR simulator into the Grand Theft Auto V game to train the method, achieving higher segmentation frames than common LiDAR sensors (10 Hz). This method was later improved to handle real point clouds [139]. Despite the real point clouds presenting more noise than the simulated ones, SqueezeSegV2 could achieve good results. Concerning the volumetric-based methods, VV-Net [140] proposed a novel approach to voxel representation. Traditionally, 3D voxel representations fail to capture the sparsely distributed points within voxels, slowing down the CNN. However, VV-Net fills this gap by using a kernel-based interpolated variational autoencoder (VAE) architecture to encode the local geometry within each voxel. Then, radial basis functions (RBF) are employed.

Regarding CNN-based object detection algorithms, they are typically defined by the number of required stages for detecting and classifying objects. Standard CNN object detection techniques rely on a two-stage method [141]. In the first step, several potential regions are proposed. Then, the category label is determined based on feature extraction for each region. Despite these approaches achieving great performance, the typical two-stage pipeline is not suitable for real-time applications due to low frame rates [149]. With the real-time requirements in mind, single-stage detection mechanisms were proposed, e.g., BirdNet [142], VoxelNet [63], and Complex-YOLO [143]. They all present interesting results despite structuring the point cloud into two different types. VoxelNet [63] provides a generic 3D detection network that extracts the object features from the point cloud structured in a 3D voxel grid. Nonetheless, the processing speed is penalized due to the sparsity of voxels typically present in the point cloud. To tackle this, both BirdNet and Complex-YOLO project the point cloud into a 2.5D view, commonly named Bird's Eye View (BEV), which is a very efficient projection for using NNs. Despite achieving faster frame rates than the other methods, e.g., Complex-YOLO can achieve real-time processing with 50fps, the performance is affected by information loss issues and by the lack of the second stage step.

## IX. Closing Discussion and Conclusion

Triggered by the automotive sector, the LiDAR market is growing at a breathtaking pace, where new players are continuously striving to develop and create new products. Since autonomous driving is becoming mainstream, LiDAR shifted to the spotlight as it is one of the most prominent solutions for achieving full awareness of the vehicle's surroundings. By today, there are already more than one hundred companies developing 3D solutions for ADAS, offering more than 150 products currently available in a market led by China and the USA [150]. Just in 2019, twenty-five automotive LiDAR start-ups achieved funding of at least USD 10 million, offering a wide set of novel imaging architectures and measuring techniques.

Aiming at consolidating knowledge on the existing LiDAR technology for automotive, this article provides a survey on the most prominent products and manufacturers that best represent the technology they offer (Table I). Besides presenting commercial sensors, this survey also presents other systems that emerged to assist research around the LiDAR, such as simulators, development platforms, and chip-based solutions. Despite all the hype around autonomous driving assisted by LiDAR sensors, we are still far to achieve systems that can easily detect and classify objects in the vehicle's surroundings. On-going research struggles to find solutions to the main LiDAR challenges that are currently hampering the development of bullet-proof solutions (summarized in Table II), such as sensor calibration, mutual interference, data compression, point cloud denoising, ground segmentation, and object segmentation and detection methods. It is expected for the upcoming years, new approaches that can easily mitigate these challenges towards great autonomous driving solutions, and LiDAR will surely leave its mark.

## References

[1] E. O. Hulburt, "Observations of a searchlight beam to an altitude of 28 kilometers," *J. Opt. Soc. Amer.*, vol. 27, no. 11, pp. 377–382, Nov. 1937.
[2] W. E. K. Middleton and A. F. Spilhaus, "Meteorological instruments," *Quart. J. Roy. Meteorol. Soc.*, vol. 80, no. 345, p. 484, 1954.
[3] J. Ring, "The laser in astronomy," *New Scientist*, vol. 18, no. 344, pp. 672–673, 1963.
[4] T. H. Maiman, "Stimulated optical radiation in ruby," *Nature*, vol. 187, no. 4736, pp. 493–494, Aug. 1960.
[5] R. O. Dubayah and J. B. Drake, "LiDAR remote sensing for forestry," *J. Forestry*, vol. 98, no. 6, pp. 44–46, Jun. 2000.
[6] E. D. Hinkley, *Laser Monitoring of the Atmosphere*. Berlin, Germany: Springer-Verlag, 1976.
[7] W. Claus, *Lidar: Range-Resolved Optical Remote Sensing of the Atmosphere*. New York, NY, USA: Springer, Jun. 2006.
[8] J. Shan and C. K. Toth, *Topographic Laser Ranging and Scanning: Principles and Processing*. Boca Raton, FL, USA: CRC Press, 2018.
[9] S. P. Healey, P. L. Patterson, S. Saatchi, M. A. Lefsky, A. J. Lister, and E. A. Freeman, "A sample design for globally consistent biomass estimation using LiDAR data from the geoscience laser altimeter system (GLAS)," *Carbon Balance Manage.*, vol. 7, no. 1, p. 10, Dec. 2012.
[10] J. E. Kay *et al.*, "Evaluating and improving cloud phase in the community atmosphere model version 5 using spaceborne LiDAR observations," *J. Geophys. Res., Atmos.*, vol. 121, no. 8, pp. 4162–4176, Apr. 2016.
[11] U. Weiss and P. Biber, "Plant detection and mapping for agricultural robots using a 3D LiDAR sensor," *Robot. Auton. Syst.*, vol. 59, no. 5, pp. 265–273, May 2011.
[12] M. Buehler, K. Iagnemma, and S. Singh, *The DARPA Urban Challenge: Autonomous Vehicles in City Traffic*, 1st ed. Springer, 2009.
[13] C. Urmson *et al.*, "High speed navigation of unrehearsed terrain: Red team technology for grand challenge 2004," Robot. Inst., Carnegie Mellon Univ., Pittsburgh, PA, USA, Tech. Rep. CMU-RI-04-37, Jan. 2004.
[14] S. Thrun *et al.*, "Stanley: The robot that won the DARPA grand challenge," *J. Field Robot.*, vol. 23, pp. 661–692, Jan. 2006.
[15] J. Guerrero-Ibáñez, S. Zeadally, and J. Contreras-Castillo, "Sensor technologies for intelligent transportation systems," *Sensors*, vol. 18, no. 4, p. 1212, Apr. 2018.
[16] E. Marti, M. A. de Miguel, F. Garcia, and J. Perez, "A review of sensor technologies for perception in automated driving," *IEEE Intell. Transp. Syst. Mag.*, vol. 11, no. 4, pp. 94–108, Sep. 2019.
[17] B. S. Jahromi, T. Tulabandhula, and S. Cetin, "Real-time hybrid multi-sensor fusion framework for perception in autonomous vehicles," *Sensors*, vol. 19, no. 20, p. 4357, Oct. 2019.
[18] A. S. Mohammed, A. Amamou, F. K. Ayevide, S. Kelouwani, K. Agbossou, and N. Zioui, "The perception system of intelligent ground vehicles in all weather conditions: A systematic literature review," *Sensors*, vol. 20, no. 22, p. 6532, Nov. 2020.
[19] D. K. Barton, "Radar system analysis and modeling," *IEEE Aerosp. Electron. Syst. Mag.*, vol. 20, no. 4, pp. 23–25, Apr. 2005.
[20] M. Richards, J. Scheer, and W. Holm, *Principles of Modern Radar: Basic Principles*. London, U.K.: Institution of Engineering and Technology, Jan. 2010.
[21] H. Wang, B. Wang, B. Liu, X. Meng, and G. Yang, "Pedestrian recognition and tracking using 3D LiDAR for autonomous vehicle," *Robot. Auton. Syst.*, vol. 88, pp. 71–78, Feb. 2017.

[22] M. Murad *et al.*, "Requirements for next generation automotive radars," in *Proc. IEEE Radar Conf. (RadarCon)*, Apr. 2013, pp. 1–6.

[23] M.-C. Amann, T. Bosch, M. Lescure, R. Myllyla, and M. Rioux, "Laser ranging: A critical review of usual techniques for distance measurement," *Opt. Eng.*, vol. 40, no. 1, pp. 10–19, 2001.

[24] D. J. Lum, "Ultrafast time-of-flight 3D LiDAR," *Nature Photon.*, vol. 14, no. 1, pp. 2–4, Jan. 2020.

[25] B. Behroozpour, P. A. M. Sandborn, M. C. Wu, and B. E. Boser, "LiDAR system architectures and circuits," *IEEE Commun. Mag.*, vol. 55, no. 10, pp. 135–142, Oct. 2017.

[26] J. Lambert *et al.*, "Performance analysis of 10 models of 3D LiDARs for automated driving," *IEEE Access*, vol. 8, pp. 131699–131722, 2020.

[27] C. Rablau, "LiDAR: A new self-driving vehicle for introducing optics to broader engineering and non-engineering audiences," in *Proc. 15th Conf. Educ. Training Opt. Photon. (ETOP)*, vol. 11143, A.-S. Poulin-Girard and J. A. Shaw, Eds. Bellingham, WA, USA: SPIE, 2019, pp. 84–97.

[28] M. E. Warren, "Automotive LiDAR technology," in *Proc. Symp. VLSI Circuits*, Jun. 2019, pp. C254–C255.

[29] J. Wojtanowski, M. Zygmunt, M. Kaszczuk, Z. Mierczyk, and M. Muzal, "Comparison of 905 nm and 1550 nm semiconductor laser rangefinders' performance deterioration due to adverse environmental conditions," *Opto-Electron. Rev.*, vol. 22, no. 3, pp. 183–190, Jan. 2014.

[30] J. Liu, Q. Sun, Z. Fan, and Y. Jia, "TOF LiDAR development in autonomous vehicle," in *Proc. IEEE 3rd Optoelectron. Global Conf. (OGC)*, Sep. 2018, pp. 185–190.

[31] S. Royo and M. Ballesta-Garcia, "An overview of LiDAR imaging systems for autonomous vehicles," *Appl. Sci.*, vol. 9, no. 19, p. 4093, Sep. 2019.

[32] Y. Li and J. Ibanez-Guzman, "LiDAR for autonomous driving: The principles, challenges, and trends for automotive LiDAR and perception systems," *IEEE Signal Process. Mag.*, vol. 37, no. 4, pp. 50–61, Jul. 2020.

[33] R. Machado, J. Cabral, and F. S. Alves, "Recent developments and challenges in FPGA-based time-to-digital converters," *IEEE Trans. Instrum. Meas.*, vol. 68, no. 11, pp. 4205–4221, Nov. 2019.

[34] T. Fersch, R. Weigel, and A. Koelpin, "A CDMA modulation technique for automotive time-of-flight LiDAR systems," *IEEE Sensors J.*, vol. 17, no. 11, pp. 3507–3516, Jun. 2017.

[35] M. Koskinen, J. T. Kostamovaara, and R. A. Myllylae, "Comparison of continuous-wave and pulsed time-of-flight laser range-finding techniques," *Proc. SPIE*, vol. 1614, pp. 296–305, Mar. 1992.

[36] A. Suss, V. Rochus, M. Rosmeulen, and X. Rottenberg, "Benchmarking time-of-flight based depth measurement techniques," in *Proc. 18th Smart Photon. Optoelectron. Integr. Circuits*, vol. 9751, S. He, E.-H. Lee, and L. A. Eldada, Eds. Bellingham, WA, USA: SPIE, 2016, pp. 199–217.

[37] A. Jelalian, "Laser radar systems," in *Proc. Electron. Aerosp. Syst. Conf. (EASCON)*, Jan. 1980, pp. 546–554.

[38] R. Agishev, B. Gross, F. Moshary, A. Gilerson, and S. Ahmed, "Range-resolved pulsed and CWFM LiDARs: Potential capabilities comparison," *Appl. Phys. B*, vol. 85, no. 1, pp. 149–162, Oct. 2006.

[39] T. Raj, F. H. Hashim, A. B. Huddin, M. F. Ibrahim, and A. Hussain, "A survey on LiDAR scanning mechanisms," *Electronics*, vol. 9, no. 5, p. 741, Apr. 2020.

[40] R. Halterman and M. Bruch, "Velodyne HDL-64E LiDAR for unmanned surface vehicle obstacle detection," *Proc. SPIE*, vol. 7692, p. 9, Apr. 2010.

[41] S. T. S. Holmström, U. Baran, and H. Urey, "MEMS laser scanners: A review," *J. Microelectromech. Syst.*, vol. 23, no. 2, pp. 259–275, Apr. 2014.

[42] H. W. Yoo *et al.*, "MEMS-based LiDAR for autonomous driving," *e i Elektrotechnik und Informationstechnik*, vol. 135, no. 6, pp. 408–415, Oct. 2018.

[43] V. Milanović, A. Kasturi, H. J. Kim, and F. Hu, "Iterative learning control algorithm for greatly increased bandwidth and linearity of MEMS mirrors in LiDAR and related imaging applications," in *Proc. 17th MOEMS Miniaturized Syst.*, vol. 10545, W. Piyawattanametha, Y.-H. Park, and H. Zappe, Eds. Bellingham, WA, USA: SPIE, 2018, pp. 242–256.

[44] B. L. Stann, J. F. Dammann, and M. M. Giza, "Progress on MEMS-scanned ladar," in *Proc. 21st Laser Radar Technol. Appl.*, vol. 9832, M. D. Turner and G. W. Kamerman, Eds. Bellingham, WA, USA: SPIE, 2016, pp. 197–205.

[45] D. Wang, C. Watkins, and H. Xie, "MEMS mirrors for LiDAR: A review," *Micromachines*, vol. 11, no. 5, p. 456, Apr. 2020.

[46] M. J. Heck, "Highly integrated optical phased arrays: Photonic integrated circuits for optical beam shaping and beam steering," *Nanophotonics*, vol. 6, no. 1, p. 152, Jan. 2017.

[47] R. Fatemi, B. Abiri, A. Khachaturian, and A. Hajimiri, "High sensitivity active flat optics optical phased array receiver with a two-dimensional aperture," *Opt. Exp.*, vol. 26, no. 23, pp. 29983–29999, Nov. 2018.

[48] C. V. Poulton *et al.*, "Long-range LiDAR and free-space data communication with high-performance optical phased arrays," *IEEE J. Sel. Topics Quantum Electron.*, vol. 25, no. 5, pp. 1–8, Sep. 2019.

[49] C.-P. Hsu *et al.*, "A review and perspective on optical phased array for automotive LiDAR," *IEEE J. Sel. Topics Quantum Electron.*, vol. 27, no. 1, pp. 1–16, Jan. 2021.

[50] S. Chung, M. Nakai, S. Idres, Y. Ni, and H. Hashemi, "19.1 optical phased-array FMCW LiDAR with on-chip calibration," in *IEEE Int. Solid-State Circuits Conf. (ISSCC) Dig. Tech. Papers*, Feb. 2021, pp. 286–288.

[51] J. Lemmetti, N. Sorri, I. Kallioniemi, P. Melanen, and P. Uusimaa, "Long-range all-solid-state flash LiDAR sensor for autonomous driving," *Proc. SPIE*, vol. 11668, Mar. 2021, Art. no. 116680P.

[52] C. Zhang, S. Lindner, I. M. Antolović, J. M. Pavia, M. Wolf, and E. Charbon, "A 30-frames/s, 252 × 144 SPAD flash LiDAR with 1728 dual-clock 48.8-ps TDCs, and pixel-wise integrated histogramming," *IEEE J. Solid-State Circuits*, vol. 54, no. 4, pp. 1137–1151, Apr. 2019.

[53] J. Hu, B. Liu, R. Ma, M. Liu, and Z. Zhu, "A 32×32-pixel flash LiDAR sensor with noise filtering for high-background noise applications," *IEEE Trans. Circuits Syst. I, Reg. Papers*, early access, Jan. 12, 2021.

[54] C. H. Jang, C. S. Kim, K. C. Jo, and M. Sunwoo, "Design factor optimization of 3D flash LiDAR sensor based on geometrical model for automated vehicle and advanced driver assistance system applications," *Int. J. Automot. Technol.*, vol. 18, no. 1, pp. 147–156, Feb. 2017.

[55] Q. Gong *et al.*, *Advances in Nanophotonics*. Berlin, Germany: De Gruyter, 2014.

[56] M. Dummer, K. Johnson, S. Rothwell, K. Tatah, and M. Hibbs-Brenner, "The role of VCSELs in 3D sensing and LiDAR," in *Proc. 21 Opt. Interconnects*, vol. 11692, H. Schröder and R. T. Chen, Eds. Bellingham, WA, USA: SPIE, 2021, pp. 42–55.

[57] *LCA2 LeddarEngine—SoC and Software for the Autoand Mobility LiDAR Platform, Version 1*, LeddarTech, 2019.

[58] ACozma, *AD-FMCLIDAR1-EBZ User Guide, Version 1*, Analog Devices, 2019.

[59] AEye. *AEye iDAR*. Accessed: Apr. 20, 2021. [Online]. Available: https://www.aeye.ai/idar/

[60] *Apollo*. Accessed: Apr. 20, 2021. [Online]. Available: https://apollo.auto/developer.html

[61] *rFpro*. Accessed: Apr. 20, 2021. [Online]. Available: http://www.rfpro.com

[62] *AAI—Sensor Simulation*. Accessed: Apr. 20, 2021. [Online]. Available: https://www.automotive-ai.com

[63] Y. Zhou and O. Tuzel, "VoxelNet: End-to-end learning for point cloud based 3D object detection," in *Proc. IEEE/CVF Conf. Comput. Vis. Pattern Recognit.*, Jun. 2018, pp. 4490–4499.

[64] J. Fang *et al.*, "Augmented LiDAR simulator for autonomous driving," *IEEE Robot. Autom. Lett.*, vol. 5, no. 2, pp. 1931–1938, Apr. 2020.

[65] C. Goodin, D. Carruth, M. Doude, and C. Hudson, "Predicting the influence of rain on LiDAR in ADAS," *Electronics*, vol. 8, no. 1, p. 89, Jan. 2019.

[66] G. Atanacio-Jiménez *et al.*, "LiDAR velodyne HDL-64E calibration using pattern planes," *Int. J. Adv. Robot. Syst.*, vol. 8, no. 5, p. 59, Nov. 2011.

[67] R. Bergelt, O. Khan, and W. Hardt, "Improving the intrinsic calibration of a velodyne LiDAR sensor," in *Proc. IEEE SENSORS*, Oct. 2017, pp. 1–3.

[68] N. Muhammad and S. Lacroix, "Calibration of a rotating multi-beam LiDAR," in *Proc. IEEE/RSJ Int. Conf. Intell. Robots Syst.*, Oct. 2010, pp. 5648–5653.

[69] C. Glennie and D. D. Lichti, "Static calibration and analysis of the velodyne HDL-64E S2 for high accuracy mobile scanning," *Remote Sens.*, vol. 2, no. 6, pp. 1610–1624, Jun. 2010.

[70] L.-J. Li, W. Chen, X.-Y. Zhao, and M.-J. Sun, "Fast optical phased array calibration technique for random phase modulation LiDAR," *IEEE Photon. J.*, vol. 11, no. 1, pp. 1–10, Feb. 2019.

[71] D.-H. Kim and G.-W. Kim, "Efficient calibration method of multiple LiDARs on autonomous vehicle platform," in *Proc. IEEE Int. Conf. Big Data Smart Comput. (BigComp)*, Feb. 2020, pp. 446–447.

[72] J. Kim, C. Kim, and H. J. Kim, "Robust extrinsic calibration for arbitrarily configured dual 3D LiDARs using a single planar board," in *Proc. 20th Int. Conf. Control, Automat. Syst. (ICCAS)*, Oct. 2020, pp. 576–580.

[73] N. Heide, T. Emter, and J. Petereit, "Calibration of multiple 3D LiDAR sensors to a common vehicle frame," in *Proc. 50th Int. Symp. Robot. (ISR)*, Jun. 2018, pp. 1–8.

[74] Y. Lyu, L. Bai, M. Elhousni, and X. Huang, "An interactive LiDAR to camera calibration," in *Proc. IEEE High Perform. Extreme Comput. Conf. (HPEC)*, Sep. 2019, pp. 1–6.

[75] Z. Pusztai, I. Eichhardt, and L. Hajder, "Accurate calibration of multi-LiDAR-multi-camera systems," *Sensors*, vol. 18, no. 7, p. 2139, Jul. 2018.

[76] C. Guindel, J. Beltran, D. Martin, and F. Garcia, "Automatic extrinsic calibration for LiDAR-stereo vehicle sensor setups," in *Proc. IEEE 20th Int. Conf. Intell. Transp. Syst. (ITSC)*, Oct. 2017, pp. 1–6.

[77] M. A. Muñoz-Bañón, F. A. Candelas, and F. Torres, "Targetless camera-LiDAR calibration in unstructured environments," *IEEE Access*, vol. 8, p. 143692–143705, 2020.

[78] L. Tamas and Z. Kato, "Targetless calibration of a LiDAR-perspective camera pair," in *Proc. IEEE Int. Conf. Comput. Vis. Workshops*, Dec. 2013, pp. 668–675.

[79] S. Bileschi, "Fully automatic calibration of LiDAR and video streams from a vehicle," in *Proc. IEEE 12th Int. Conf. Comput. Vis. Workshops, ICCV Workshops*, Sep. 2009, pp. 1457–1464.

[80] C. Park, P. Moghadam, S. Kim, S. Sridharan, and C. Fookes, "Spatiotemporal camera-LiDAR calibration: A targetless and structureless approach," *IEEE Robot. Autom. Lett.*, vol. 5, no. 2, pp. 1556–1563, Apr. 2020.

[81] C. Chen, G. Xiong, Z. Zhang, J. Gong, J. Qi, and C. Wang, "3D LiDAR-GPS/IMU calibration based on hand-eye calibration model for unmanned vehicle," in *Proc. 3rd Int. Conf. Unmanned Syst. (ICUS)*, Nov. 2020, pp. 337–341.

[82] G. Kim, J. Eom, and Y. Park, "An experiment of mutual interference between automotive LiDAR scanners," in *Proc. 12th Int. Conf. Inf. Technol.-New Generat.*, Apr. 2015, pp. 680–685.

[83] J. Eom, G. Kim, and Y. Park, "Mutual interference potential and impact of scanning LiDAR according to the relevant vehicle applications," in *Proc. 24th Laser Radar Technol. Appl.*, vol. 11005, M. D. Turner and G. W. Kamerman, Eds. Bellingham, WA, USA: SPIE, 2019, pp. 133–142.

[84] I.-P. Hwang, S.-J. Yun, and C.-H. Lee, "Study on the frequency-modulated continuous-wave LiDAR mutual interference," in *Proc. IEEE 19th Int. Conf. Commun. Technol. (ICCT)*, Oct. 2019, pp. 1053–1056.

[85] I.-P. Hwang, S.-J. Yun, and C.-H. Lee, "Mutual interferences in frequency-modulated continuous-wave (FMCW) LiDARs," *Optik*, vol. 220, Oct. 2020, Art. no. 165109.

[86] I.-P. Hwang and C.-H. Lee, "A rapid LiDAR without mutual interferences," in *Proc. Opt. Fiber Commun. Conf. (OFC)*, 2019, pp. 1–3, Paper M2J.4.

[87] I. Hwang and C. Lee, "Mutual interferences of a true-random LiDAR with other LiDAR signals," *IEEE Access*, vol. 8, pp. 124123–124133, 2020.

[88] I. Maksymova, C. Steger, and N. Druml, "Review of LiDAR sensor data acquisition and compression for automotive applications," *Proceedings*, vol. 2, no. 13, p. 852, Dec. 2018.

[89] D. Graziosi, O. Nakagami, S. Kuma, A. Zaghetto, T. Suzuki, and A. Tabatabai, "An overview of ongoing point cloud compression standardization activities: Video-based (V-PCC) and geometry-based (G-PCC)," *APSIPA Trans. Signal Inf. Process.*, vol. 9, p. e13, Apr. 2020.

[90] P. Caillet and Y. Dupuis, "Efficient LiDAR data compression for embedded V2I or V2V data handling," *ArXiv*, vol. abs/1904.05649, pp. 1–6, 2019

[91] M. M. Abdelwahab, W. S. El-Deeb, and A. A. A. Youssif, "LiDAR data compression challenges and difficulties," in *Proc. 5th Int. Conf. Frontiers Signal Process. (ICFSP)*, Sep. 2019, pp. 111–116.

[92] M. Isenburg, "LASzip: Lossless compression of LiDAR data," *Photogramm. Eng. Remote Sens.*, vol. 79, pp. 209–217, Feb. 2013.

[93] D. Mongus and B. Žalik, "Efficient method for lossless LiDAR data compression," *Int. J. Remote Sens.*, vol. 32, no. 9, pp. 2507–2518, May 2011.

[94] T. Golla and R. Klein, "Real-time point cloud compression," in *Proc. IEEE/RSJ Int. Conf. Intell. Robots Syst. (IROS)*, Sep. 2015, pp. 5087–5092.

[95] C. Tu, E. Takeuchi, A. Carballo, and K. Takeda, "Real-time streaming point cloud compression for 3D LiDAR sensor using U-Net," *IEEE Access*, vol. 7, pp. 113616–113625, 2019.

[96] J. Kammerl, N. Blodow, R. B. Rusu, S. Gedikli, M. Beetz, and E. Steinbach, "Real-time compression of point cloud streams," in *Proc. IEEE Int. Conf. Robot. Automat.*, May 2012, pp. 778–785.

[97] P. V. Beek, "Image-based compression of LiDAR sensor data," *Electron. Imag.*, vol. 2019, no. 15, pp. 43-1–43-7, 2019.

[98] H. Houshiar and A. Nuchter, "3D point cloud compression using conventional image compression for efficient data transmission," in *Proc. 25th Int. Conf. Inf., Commun. Automat. Technol. (ICAT)*, Oct. 2015, pp. 1–8.

[99] A. M. Wallace, A. Halimi, and G. S. Buller, "Full waveform LiDAR for adverse weather conditions," *IEEE Trans. Veh. Technol.*, vol. 69, no. 7, pp. 7064–7077, Jul. 2020.

[100] N. Charron, S. Phillips, and S. L. Waslander, "De-noising of LiDAR point clouds corrupted by snowfall," in *Proc. 15th Conf. Comput. Robot Vis. (CRV)*, May 2018, pp. 254–261.

[101] P. H. Chan, G. Dhadyalla, and V. Donzella, "A framework to analyze noise factors of automotive perception sensors," *IEEE Sensors Lett.*, vol. 4, no. 6, pp. 1–4, Jun. 2020.

[102] H. Balta, J. Velagic, W. Bosschaerts, G. De Cubber, and B. Siciliano, "Fast statistical outlier removal based method for large 3D point clouds of outdoor environments," *IFAC-PapersOnLine*, vol. 51, no. 22, pp. 348–353, 2018.

[103] J. I. Park, J. Park, and K. S. Kim, "Fast and accurate desnowing algorithm for LiDAR point clouds," *IEEE Access*, vol. 8, pp. 160202–160212, 2020.

[104] R. Heinzler, F. Piewak, P. Schindler, and W. Stork, "CNN-based LiDAR point cloud de-noising in adverse weather," *IEEE Robot. Autom. Lett.*, vol. 5, no. 2, pp. 2514–2521, Apr. 2020.

[105] X. Meng, Z. Cao, S. Liang, L. Pang, S. Wang, and C. Zhou, "A terrain description method for traversability analysis based on elevation grid map," *Int. J. Adv. Robot. Syst.*, vol. 15, no. 1, pp. 1–12, 2018.

[106] Q. Li *et al.*, "Motion field estimation for a dynamic scene using a 3D LiDAR," *Sensors*, vol. 14, no. 9, pp. 16672–16691, 2014. [Online]. Available: https://www.mdpi.com/1424-8220/14/9/16672

[107] M. Himmelsbach, F. V. Hundelshausen, and H.-J. Wuensche, "Fast segmentation of 3D point clouds for ground vehicles," in *Proc. IEEE Intell. Vehicles Symp.*, Jun. 2010, pp. 560–565.

[108] T. Chen, B. Dai, D. Liu, and J. Song, "Sparse Gaussian process regression based ground segmentation for autonomous land vehicles," in *Proc. 27th Chin. Control Decis. Conf. (CCDC)*, May 2015, pp. 3993–3998.

[109] T. Chen, B. Dai, R. Wang, and D. Liu, "Gaussian-process-based real-time ground segmentation for autonomous land vehicles," *J. Intell. Robot. Syst.*, vol. 76, nos. 3–4, pp. 563–582, Dec. 2014.

[110] K. Liu, W. Wang, R. Tharmarasa, J. Wang, and Y. Zuo, "Ground surface filtering of 3D point clouds based on hybrid regression technique," *IEEE Access*, vol. 7, pp. 23270–23284, 2019.

[111] Z. Cheng, G. Ren, and Y. Zhang, "Ground segmentation algorithm based on 3D LiDAR point cloud," in *Proc. Int. Conf. Mech., Electr., Electron. Eng. Sci. (MEEES)*, 2018, pp. 16–21.

[112] S. Xu, R. Wang, H. Wang, and H. Zheng, "An optimal hierarchical clustering approach to mobile LiDAR point clouds," *IEEE Trans. Intell. Transp. Syst.*, vol. 21, no. 7, pp. 2765–2776, Jul. 2020.

[113] S. Xu, R. Wang, H. Wang, and R. Yang, "Plane segmentation based on the optimal-vector-field in LiDAR point clouds," *IEEE Trans. Pattern Anal. Mach. Intell.*, early access, May 18, 2020.

[114] J. Serafin, E. Olson, and G. Grisetti, "Fast and robust 3D feature extraction from sparse point clouds," in *Proc. IEEE/RSJ Int. Conf. Intell. Robots Syst. (IROS)*, Oct. 2016, pp. 4105–4112.

[115] R. B. Rusu, A. Holzbach, N. Blodow, and M. Beetz, "Fast geometric point labeling using conditional random fields," in *Proc. IEEE/RSJ Int. Conf. Intell. Robots Syst.*, Oct. 2009, pp. 7–12.

[116] L. Rummelhard, A. Paigwar, A. Nègre, and C. Laugier, "Ground estimation and point cloud segmentation using spatiotemporal conditional random field," in *Proc. IEEE Intell. Vehicles Symp. (IV)*, Jun. 2017, pp. 1105–1110.

[117] C. Guo, W. Sato, L. Han, S. Mita, and D. McAllester, "Graph-based 2D road representation of 3D point clouds for intelligent vehicles," in *Proc. IEEE Intell. Vehicles Symp. (IV)*, Jun. 2011, pp. 715–721.

[118] J. Byun, K.-I. Na, B.-S. Seo, and M. Roh, *Drivable Road Detection With 3D Point Clouds Based on the MRF for Intelligent Vehicle*. Cham, Switzerland: Springer, 2015, pp. 49–60.

[119] M. Zhang, D. D. Morris, and R. Fu, "Ground segmentation based on loopy belief propagation for sparse 3D point clouds," in *Proc. Int. Conf. 3D Vis.*, Oct. 2015, pp. 615–622.

[120] W. Huang *et al.*, "A fast point cloud ground segmentation approach based on coarse-to-fine Markov random field," *IEEE Trans. Intell. Transp. Syst.*, early access, Apr. 21, 2021.

[121] L. Landrieu and M. Simonovsky, "Large-scale point cloud semantic segmentation with superpoint graphs," in *Proc. IEEE/CVF Conf. Comput. Vis. Pattern Recognit.*, Jun. 2018, pp. 4558–4567.

[122] Z. Zhang, B.-S. Hua, and S.-K. Yeung, "ShellNet: Efficient point cloud convolutional neural networks using concentric shells statistics," in *Proc. IEEE/CVF Int. Conf. Comput. Vis. (ICCV)*, Oct. 2019, pp. 1607–1616.

[123] Q. Hu *et al.*, "RandLA-Net: Efficient semantic segmentation of large-scale point clouds," in *Proc. IEEE/CVF Conf. Comput. Vis. Pattern Recognit. (CVPR)*, Jun. 2020, pp. 11108–11117.

[124] Z. Luo, M. V. Mohrenschildt, and S. Habibi, "A probability occupancy grid based approach for real-time LiDAR ground segmentation," *IEEE Trans. Intell. Transp. Syst.*, vol. 21, no. 3, pp. 998–1010, Mar. 2020.

[125] M. Velas, M. Spanel, M. Hradis, and A. Herout, "CNN for very fast ground segmentation in velodyne LiDAR data," in *Proc. IEEE Int. Conf. Auton. Robot Syst. Competitions (ICARSC)*, Apr. 2018, pp. 97–103.

[126] E. Romera, J. M. Álvarez, L. M. Bergasa, and R. Arroyo, "ERFNet: Efficient residual factorized ConvNet for real-time semantic segmentation," *IEEE Trans. Intell. Transp. Syst.*, vol. 19, no. 1, pp. 263–272, Jan. 2018.

[127] C. Lee and J.-H. Moon, "Robust lane detection and tracking for real-time applications," *IEEE Trans. Intell. Transp. Syst.*, vol. 19, no. 12, pp. 4043–4048, Dec. 2018.

[128] J. Zhang and S. Singh, "LOAM: LiDAR odometry and mapping in real-time," in *Proc. Robot., Sci. Syst.*, Berkeley, CA, USA, Jul. 2014, pp. 1–9.

[129] P. Agrawal, A. Iqbal, B. Russell, M. K. Hazrati, V. Kashyap, and F. Akhbari, "PCE-SLAM: A real-time simultaneous localization and mapping using LiDAR data," in *Proc. IEEE Intell. Vehicles Symp. (IV)*, Jun. 2017, pp. 1752–1757.

[130] J.-E. Deschaud, "IMLS-SLAM: Scan-to-model matching based on 3D data," in *Proc. IEEE Int. Conf. Robot. Autom. (ICRA)*, May 2018, pp. 2480–2485.

[131] J. Li, J. Zhao, Y. Kang, X. He, C. Ye, and L. Sun, "DL-SLAM: Direct 2.5D LiDAR SLAM for autonomous driving," in *Proc. IEEE Intell. Vehicles Symp. (IV)*, Jun. 2019, pp. 1205–1210.

[132] D. Rozenberszki and A. L. Majdik, "LOL: LiDAR-only odometry and localization in 3D point cloud maps," in *Proc. IEEE Int. Conf. Robot. Automat. (ICRA)*, May 2020, pp. 4379–4385.

[133] K. Yilmaz, B. Suslu, S. Roychowdhury, and L. S. Muppirisetty, "AV-SLAM: Autonomous vehicle SLAM with gravity direction initialization," in *Proc. 25th Int. Conf. Pattern Recognit. (ICPR)*, Jan. 2021, pp. 8093–8100.

[134] W. Lu, Y. Zhou, G. Wan, S. Hou, and S. Song, "L3-Net: Towards learning based LiDAR localization for autonomous driving," in *Proc. IEEE/CVF Conf. Comput. Vis. Pattern Recognit. (CVPR)*, Jun. 2019, pp. 6382–6391.

[135] R. Q. Charles, H. Su, M. Kaichun, and L. J. Guibas, "PointNet: Deep learning on point sets for 3D classification and segmentation," in *Proc. IEEE Conf. Comput. Vis. Pattern Recognit. (CVPR)*, Jul. 2017, pp. 77–85.

[136] C. R. Qi, L. Yi, H. Su, and L. J. Guibas, "PointNet++: Deep hierarchical feature learning on point sets in a metric space," in *Proc. Adv. Neural Inf. Process. Syst.*, 2017, pp. 5099–5108.

[137] S. Shi, X. Wang, and H. Li, "PointRCNN: 3D object proposal generation and detection from point cloud," in *Proc. IEEE/CVF Conf. Comput. Vis. Pattern Recognit. (CVPR)*, Jun. 2019, pp. 770–779.

[138] B. Wu, A. Wan, X. Yue, and K. Keutzer, "SqueezeSeg: Convolutional neural nets with recurrent CRF for real-time road-object segmentation from 3D LiDAR point cloud," in *Proc. IEEE Int. Conf. Robot. Automat. (ICRA)*, May 2018, pp. 1887–1893.

[139] B. Wu, X. Zhou, S. Zhao, X. Yue, and K. Keutzer, "SqueezeSegV2: Improved model structure and unsupervised domain adaptation for road-object segmentation from a LiDAR point cloud," in *Proc. Int. Conf. Robot. Automat. (ICRA)*, May 2019, pp. 4376–4382.

[140] H.-Y. Meng, L. Gao, Y.-K. Lai, and D. Manocha, "VV-Net: Voxel VAE net with group convolutions for point cloud segmentation," in *Proc. IEEE/CVF Int. Conf. Comput. Vis. (ICCV)*, Oct. 2019, pp. 8500–8508.

[141] Z. Yang, Y. Sun, S. Liu, X. Shen, and J. Jia, "STD: Sparse-to-dense 3D object detector for point cloud," in *Proc. IEEE/CVF Int. Conf. Comput. Vis. (ICCV)*, Oct. 2019, pp. 1951–1960.

[142] J. Beltrán, C. Guindel, F. M. Moreno, D. Cruzado, F. García, and A. De La Escalera, "BirdNet: A 3D object detection framework from LiDAR information," in *Proc. 21st Int. Conf. Intell. Transp. Syst. (ITSC)*, Nov. 2018, pp. 3517–3523.

[143] M. Simon, S. Milz, K. Amende, and H. Gross, "Complex-YOLO: Real-time 3D object detection on point clouds," *arXiv*, vol. abs/1803.06199, pp. 1–14, 2018.

[144] D. Z. Wang and I. Posner, "Voting for voting in online point cloud object detection," in *Proc. Robot., Sci. Syst.*, 2015, vol. 1, no. 3, p. 15607.

[145] M. Himmelsbach, T. Luettel, and H.-J. Wuensche, "Real-time object classification in 3D point clouds using point feature histograms," in *Proc. IEEE/RSJ Int. Conf. Intell. Robots Syst.*, Oct. 2009, pp. 994–1000.

[146] Y. Guo, H. Wang, Q. Hu, H. Liu, L. Liu, and M. Bennamoun, "Deep learning for 3D point clouds: A survey," *IEEE Trans. Pattern Anal. Mach. Intell.*, early access, Jun. 29, 2020.

[147] S. Grigorescu, B. Trasnea, T. Cocias, and G. Macesanu, "A survey of deep learning techniques for autonomous driving," *J. Field Robot.*, vol. 37, no. 3, pp. 362–386, Apr. 2020.

[148] E. Arnold, O. Y. Al-Jarrah, M. Dianati, S. Fallah, D. Oxtoby, and A. Mouzakitis, "A survey on 3D object detection methods for autonomous driving applications," *IEEE Trans. Intell. Transp. Syst.*, vol. 20, no. 10, pp. 3782–3795, Oct. 2019.

[149] B. Yang, W. Luo, and R. Urtasun, "PIXOR: Real-time 3D object detection from point clouds," in *Proc. IEEE/CVF Conf. Comput. Vis. Pattern Recognit. (CVPR)*, Jun. 2018, pp. 7652–7660.

[150] N. Wijeyasinghe and K. Ghaffarzadeh, "LiDAR 2020–2030: Technologies, players, markets & forecasts," IDTechEx Res., Cambridge, U.K., Tech. Rep., Oct. 2019. [Online]. Available: https://www.idtechex.com/en/research-report/lidar-2020-2030-technologies-players-markets-and-forecasts/694

**Ricardo Roriz** received the master's degree in industrial electronics and computers engineering from the University of Minho, Portugal. He is currently pursuing the Ph.D. degree in sensors and instrumentation systems for the automotive industry. He is currently an Active Research Fellow with the Embedded Systems Research Group, ALGORITMI Research Center. His research interest includes embedded systems design and robotics, with particular focus on FPGA-assisted acceleration systems.

**Jorge Cabral** received the Ph.D. degree in electrical engineering from Imperial College London. Since 2015, he has been the Deputy Director with the ALGORITMI Research Centre. He is currently with the Embedded Systems Research Group, ALGORITMI Research Centre. He is leading several projects in the field of sensors and instrumentation, wireless sensor networks, and embedded applications. His research interests include embedded systems, instrumentation, and microelectromechanical systems.

**Tiago Gomes** received the master's degree in telecommunications engineering and the Ph.D. degree in electronics and computers engineering from the University of Minho, Braga, Portugal. He is currently a Research Scientist and an Invited Professor with the University of Minho. His current research interests include embedded systems hardware/software co-design for resource constrained wireless devices, wireless protocols for low-rate wireless personal area networks, and network protocols for the Internet of Things low-end devices.